**Title:**

Red blood cells protect oxygen transport with adrenergic sodium-proton exchangers in hypoxic and hypercapnic white seabass

**Running title:**

Active protection of red blood cell pH

**Authors:**

Till S. Harter*, Alexander M. Clifford and Martin Tresguerres*

**Affiliations:**

Marine Biology Research Division, Scripps Institution of Oceanography, University of California San Diego, La Jolla, CA 92093, USA

*corresponding authors: tharter@ucsd.edu; mtresguerres@ucsd.edu

**Keywords:**

β-NHE, Slc9a1b, carbon dioxide, haemoglobin, red tide, Bohr effect, Root effect, fish

**Summary Statement:**

White seabass have highly pH-sensitive haemoglobins, but their red blood cells can actively protect oxygen transport during hypoxia and hypercapnia, conditions that occur more frequently due to a changing climate.

**Abstract:**

White seabass (*Atractoscion nobilis*) are increasingly experiencing periods of low oxygen ($O_2$; hypoxia) and high carbon dioxide ($CO_2$, hypercapnia) due to climate change and eutrophication of the coastal waters of California. Haemoglobin (Hb) is the principal $O_2$ carrier in the blood and in many teleost fishes Hb-$O_2$ binding is compromised at low pH. However, Hb is contained within red blood cells (RBC) that, in some species, regulate intracellular pH with adrenergically-stimulated sodium-proton-exchangers (β-NHE). We hypothesised that white seabass have RBC β-NHEs that protect the blood $O_2$-carrying capacity during hypoxia and hypercapnia. In a series of *in vitro* experiments, we determined the $O_2$-binding characteristics of white seabass blood, the response of RBCs to adrenergic stimulation, and quantified the protective effect of β-NHE activity on Hb-$O_2$ saturation during a hypercapnic acidosis in normoxia and hypoxia. White seabass had typical teleost Hb characteristics, with a moderate $O_2$ affinity that was highly pH-sensitive. Functional, molecular and bioinformatic data confirmed that white seabass have RBC β-NHEs, and super-resolution imaging revealed, for the first time, the subcellular location of β-NHE protein in intracellular vesicles and on the RBC membrane. The activation of RBC β-NHEs increased Hb-$O_2$ saturation by ~8% in normoxia at 1% $PCO_2$, and by ~20% in hypoxia at arterial $PCO_2$ (0.3%), but the protective effects decreased at higher $PCO_2$. Combined, these data indicate that RBC β-NHE activity in white seabass can safeguard arterial $O_2$ transport and the mechanism likely plays an important role in the fishes' physiological response to environmental hypoxia and hypercapnia.

## Introduction

White seabass (*Atractoscion nobilis*), a teleost fish species endemic to the coastal waters of California, are apex-predators with ecological significance, sought-after targets of recreational and commercial fisheries and are gaining importance in aquaculture. Their natural habitat along the kelp forests of the north-eastern Pacific is subject to strong seasonal fluctuations in water chemistry, due to the upwelling of deeper waters that are often depleted of oxygen ($O_2$; hypoxia), have a high carbon dioxide tension ($CO_2$; hypercapnia) and thus, a low pH (Frieder et al., 2012). In addition, a steadily warming climate and growing anthropogenic nutrient loading are increasing the frequency of large algae blooms ("red tides") in California's coastal waters (Van Dolah, F M, 2000). When these algae blooms wane, the microbial decomposition of their biomass, consumes $O_2$ and produces $CO_2$ and other toxic and acidic by-products of biological decay, such as hydrogen sulfide, altogether creating large hypoxic and hypercapnic zones (Diaz and Rosenberg, 2008). Species that are highly mobile may be able to avoid these areas, but for many sedentary species, survival will depend on enduring these conditions. Climate change at large is also leading to more hypoxic and acidic oceans and, over generations, some species may adapt to cope with their altered habitats (Harley et al., 2006). However, the reoccurrence of upwelling and severe algae blooms may acutely expose animals to conditions that far exceed worst-case predictions for the end of the century, creating strong selective pressures for hypoxia and hypercapnia tolerance and perhaps overwhelming the rates at which some species can adapt to climate change.

The most recent severe red tide in Southern California occurred in April-May of 2020, when the water measurements at the pier of the Scripps Institution of Oceanography (SIO) in La Jolla (CA, USA) revealed average daily dissolved $O_2$ levels of <2 mg $l^{-1}$ and pH as low as 7.06 (Clements et al, 2020). At a water temperature of 17°C and 35 ppt salinity, these values correspond to 5.3% $PO_2$ (or 40 mmHg; Boutilier et al., 1984) and 1.16% $PCO_2$ (CO2SYS software; Lewis and Wallace, 1998). Equally alarming was the prolonged duration of hypoxia, where for nine consecutive days, water $PO_2$ was below the threshold (4.6 mg $l^{-1}$) that is considered lethal for 90% of marine life (Vaquer-Sunyer and Duarte, 2008). The SIO aquatics facility is supplied with water taken in at the pier, which resulted in hypoxic and hypercapnic exposures of all research animals, despite every effort to aerate the tanks. However unfortunate, this natural experiment revealed a remarkable tolerance of white seabass to these adverse water

conditions, despite being deprived the behavioural avoidance of hypoxia that may be recruited in the wild. Therefore, the aim of the present study was to explore the $O_2$-transport capacity of white seabass with a focus on the physiological mechanisms at the level of the red blood cell (RBC) that may allow these fish to endure severe hypoxia and hypercapnia.

For obligate aerobic animals, the challenge to surviving unavoidable environmental hypoxia is balancing the uptake and delivery of $O_2$ with its consumption in the mitochondria (Hughes, 1973). Haemoglobin (Hb) is the principal $O_2$ carrier in the blood and therefore the cardiovascular $O_2$-carrying capacity is largely determined by the $O_2$-binding characteristics of Hb. As such, a higher Hb-$O_2$ affinity will favour the extraction of $O_2$ from hypoxic waters and thus, a lower Hb $P_{50}$ (the partial pressure of $O_2$ at which Hb is 50% saturated) is typically associated with hypoxia tolerance in fishes (Jensen and Weber, 1982; Mandic et al., 2009); however, whether white seabass have high-affinity Hbs that would confer some hypoxia tolerance is currently unknown.

Hb-$O_2$ binding in teleost fishes is highly pH-sensitive, where a reduction in pH decreases Hb-$O_2$ affinity via the Bohr effect (Bohr et al., 1904), and the Root effect prevents Hb from becoming fully $O_2$-saturated at low pH, even at super-atmospheric $PO_2$ (Root, 1931; Scholander and Van Dam, 1954). The reduction in Hb-$O_2$ carrying capacity due to the Root effect is physiologically significant, as it enhances the unloading of $O_2$ at the eyes and the swimbladder of teleosts, where blood is acidified locally (Damsgaard et al., 2020; Pelster, 1997; Wittenberg and Wittenberg, 1962). In contrast, during a systemic blood acidosis that may occur during exercise or hypoxia, the pH-sensitive Hbs of teleosts may fail to become fully oxygenated at the gills, decreasing the $O_2$-carrying capacity of arterial blood and leading to hypoxemia at the tissues. Thus, a combined hypoxic and hypercapnic exposure may be especially dangerous for teleosts, as a reduced availability of $O_2$ in the environment is paired with the simultaneous reduction of Hb-$O_2$ affinity via the Bohr effect at low pH; however, whether white seabass have pH-sensitive Hbs is currently unknown.

Hb is housed within RBCs that, in teleosts, may prevent systemic hypoxemia by actively regulating their intracellular pH ($pH_i$) to protect Hb-$O_2$ binding during a reduction in extracellular pH ($pH_e$). In brief, a decrease in arterial $PO_2$ or pH leads to the release of catecholamines into the blood (Randall and Perry, 1992; Tetens and Lykkeboe, 1988), which bind to a β-adrenergic receptor on the RBC membrane and activate a sodium-proton-exchanger

(β-NHE, Slc9a1b,) via the cyclic adenosine monophosphate (cAMP) pathway (Mahe et al., 1985). The extrusion of $H^+$ by the β-NHE raises $pH_i$ above the equilibrium condition, which increases Hb-$O_2$ affinity and will promote the extraction of $O_2$ from hypoxic waters (Nikinmaa, 1992). The adrenergic stimulation of RBCs also causes an influx of $Na^+$ and $Cl^-$ that leads to osmotic swelling and that has been used as a marker to determine the presence of RBC β-NHEs in fish species (Rummer et al., 2010; Shu et al., 2017). A broader phylogenetic analysis indicates that most teleosts, but not other fishes, have RBC β-NHEs (Berenbrink et al., 2005); however, whether white seabass RBCs have β-NHE activity is currently unknown.

Based on these considerations, we hypothesised that white seabass RBCs have β-NHE activity that will protect the blood $O_2$-carrying capacity during hypoxic and hypercapnic conditions. We tested this hypothesis in a series of *in vitro* experiments and predicted that: i) white seabass have a high Hb-$O_2$ affinity to maintain $O_2$ uptake under hypoxic conditions, which was addressed by generating oxygen equilibrium curves (OEC) over a range of $PO_2$; ii) white seabass display the large Bohr and Root effects that are typical of teleosts, which was addressed by generating OECs over a range of $PCO_2$, and measuring $pH_e$ and RBC $pH_i$; iii) white seabass have a RBC β-NHE, which was addressed using molecular, bioinformatic and immunocytochemical techniques to establish its presence and localisation, and by measuring RBC swelling after adrenergic stimulation and the inhibition of NHEs with amiloride; and finally iv) the adrenergic stimulation of RBC β-NHEs protects the blood $O_2$-carrying capacity during an acidosis and this effect was quantified by measuring Hb-$O_2$ saturation at increasing levels a hypercapnia in normoxia and hypoxia.

## Materials and Methods

### *Animals and husbandry*

White seabass (*A. nobilis*, Ayres 1860) were obtained from the Hubbs Sea World Research Institute (HSWRI, Carlsbad, USA) and were held indoors at the SIO aquatics facility for several months before experiments. Photoperiod was set to a 12:12 h light-dark cycle and fish were housed in large fiberglass tanks (~3.5-10 $m^3$) supplied with flow-through seawater from an inshore intake; the average water temperature at the time of experiments was 17°C. Aeration was provided to ensure normoxic conditions in all tanks (>90% air saturation of $O_2$) and these water parameters were monitored every day. All fish were fed twice a week with commercial dry pellets (Skretting; Classic Bass 9.5 mm; Stavanger, Norway) and feeding was suspended 48 h before blood sampling. The white seabass used for the determination of blood $O_2$-binding characteristics had an average weight of 1146±96 g ($N$ = 8), while those used for the β-NHE experiments had an average weight of 357±27 g ($N$ = 6). Animal husbandry and all experimental procedures were in strict compliance with the guidelines by the Institutional Animal Care and Use Committee (IACUC) and approved by the Animal Care Program at the University of California San Diego (Protocol no. S10320).

### *Blood sampling*

White seabass were moved individually into darkened boxes supplied with air and flow-through seawater, 24 h prior to blood sampling. The next day the water supply was shut off and the fish were anaesthetized by carefully pouring a diluted benzocaine solution (Fisher Scientific, Acros 150785000; Waltham, USA; concentrated stock made up in ethanol) into the box without disturbing the fish, for a final concentrations of 70 mg $l^{-1}$ benzocaine (<0.001% ethanol). After visible loss of equilibrium, fish were transferred to a surgery table, positioned ventral-side-up and their gills were perfused with water containing a maintenance dose of anaesthetic (30 mg $l^{-1}$ benzocaine). Blood sampling was by caudal puncture and 3 ml of blood were collected into a heparinized syringe. This procedure ensured minimal disturbance of the fish (Montgomery et al., 2019), which can decrease blood pH due to air-exposure (respiratory acidosis) and due to anaerobic muscle contractions during struggling (metabolic acidosis). After sampling, the fish were recovered and returned to their holding tank, and each individual was only sampled once. In the lab, the blood was centrifuged at 500 *g* for 3 min to separate the plasma from the blood cells. The plasma was collected in a bullet tube and stored over-night at 4°C. To remove any

catecholamines released during sampling, the blood cells were rinsed three times in cold Cortland's saline (in mM: NaCl 147, KCl 5.1, CaCl 1.6, $MgSO_4$ 0.9, $NaHCO_3$ 11.9, $NaH_2PO_4$ 3, glucose 5.6; adjusted to the measured plasma osmolality in white seabass of 345 mOsm and pH 7.8) and the buffy coat was aspirated generously to remove white blood cells and platelets. Finally, the pellet was re-suspended in 10 volumes of fresh saline to allow the RBCs to return to a resting state and stored aerobically on a tilt-shaker, over-night, at 17°C (Caldwell et al., 2006).

*Blood $O_2$-binding characteristics*

The next day, RBCs were rinsed with saline three times and re-suspended in their native plasma at a haematocrit of 5%; this value was chosen based on preliminary trials and yields an optic density that allows for spectrophotometric measurements of Hb-$O_2$ binding characteristics (~0.6 mM Hb). A volume of 1.4 ml of blood was loaded into a glass tonometer at 17°C and equilibrated to arterial gas tensions (21% $PO_2$, 0.3% $PCO_2$ in $N_2$) from a custom-mixed gas cylinder (Praxair; Danbury, USA). After one hour, 2 µl of blood were removed from the tonometer and loaded into the diffusion chamber of a spectrophotometric blood analyser (BOBS, Loligo Systems; Viborg, Denmark). The samples were equilibrated to increasing $PO_2$ tensions (0.5, 1, 2, 4, 8, 16 and 21% $PO_2$) from a gas mixing system (GMS, Loligo), in two-minute equilibration steps and the absorbance was recorded once every second at 190-885 nm. At the beginning and end of each run, the sample was equilibrated to high (99.7% $O_2$, 0.3% $CO_2$ in $N_2$ for 8 min) and low (0% $O_2$, 0.3% $CO_2$ in $N_2$ for 8 min) $PO_2$ conditions; for the calculation of Hb-$O_2$ saturation from raw absorbance values, it was assumed that Hb was fully oxygenated or deoxygenated under the two conditions, respectively. A $PCO_2$ of 0.3% was maintained throughout these trials to prevent RBC $pH_i$ from increasing above physiologically relevant levels and this value was chosen to match that measured in the arterial blood of rainbow trout (*Oncorhynchus mykiss*) *in vivo* (Brauner et al., 2000a). All custom gas mixtures were validated by measuring $PO_2$ with an FC-2 Oxzilla and $PCO_2$ with a CA-10 $CO_2$ analyser (Sable Systems, North Las Vegas, USA) that were calibrated daily against high purity $N_2$, air, or 5% $CO_2$ in air.

An additional 250 µl of blood were removed from the tonometer to measure blood parameters as follows. Haematocrit (Hct) was measured in triplicate in microcapillary tubes (Drummond Microcaps, 15 µl; Parkway, USA), after centrifuging at 10,000 *g* for 3 min. Hb was measured in triplicated using the cyano-methaemoglobin method (Sigma-Aldrich Drabkin's D5941; St. Louis, USA) and an extinction coefficient of 10.99 mmol $cm^{-1}$ (van Kampen and

Zijlstra, 1983). Blood pH was measured with a thermostatted microcapillary electrode at 17°C (Fisher Accumet 13-620-850; Hampton, USA; with Denver Instruments UB-10 meter; Bohemia, USA), calibrated daily against precision pH buffers (Radiometer S11M007, S1M004 and S11M002; Copenhagen, Denmark). Thereafter, the blood was centrifuged to separate plasma and RBCs and total $CO_2$ content ($TCO_2$) of the plasma was measured in triplicate with a Corning 965 (Midland, USA). The RBCs in the pellet were lysed by three freeze-thaw cycles in liquid nitrogen and $pH_i$ was measured in the lysate as described for $pH_e$ (Zeidler and Kim, 1977). After completing these measurements, the $PCO_2$ in the tonometer was increased in steps from 0.3 to 2.5% and, each time, OECs and blood parameters were measured as described above.

*RBC swelling after β-adrenergic stimulation*

After storage of blood samples over-night in saline, the RBCs were rinsed three times in fresh saline and re-suspended in their native plasma at a Hct of 25%. A volume of 1.8 ml was loaded into a tonometer and equilibrated to 3% $PO_2$ and 1% $PCO_2$ in $N_2$ at 17°C for one hour; similar hypoxic and acidotic conditions have been shown to promote β-NHE activity in other teleost species (Motais et al., 1987; Salama and Nikinmaa, 1989). After one hour, an initial subsample of blood was taken and Hct, Hb, $pH_e$ and $pH_i$ were measured as described above. Thereafter, the blood was split into aliquots of 600 µl that were loaded into individual tonometers and treated with either: i) a carrier control (0.25% dimethyl sulfoxide, DMSO; VWR BDH 1115; Radnor, USA), ii) the β-adrenergic agonist isoproterenol (ISO; Sigma I6504; 10 µM final concentration, which stimulates maximal β-NHE activity in rainbow trout; Tetens and Lykkeboe, 1988), or iii) ISO plus the NHE inhibitor amiloride (ISO+Am; Sigma A7410; 1 mM, according to Borgese et al., 1992). These treatments were staggered so that samples from each tonometer could be taken for the measurements of blood parameters at 10, 30 and 60 mins after drug additions.

To collect RBC samples for immunocytochemistry, the above tonometry trial was repeated ($N$ = 2) with RBCs that were suspended in saline instead of plasma; this step was necessary as initial trials showed that plasma proteins interfered with the quality of cell fixations. Subsamples were removed from individual tonometers at the initial and 60 min time points. A volume of 60 µl was immediately re-suspended in 1.5 ml ice-cold fixative (3% paraformaldehyde, 0.175 % glutaraldehyde in 0.6 x phosphate buffered saline with 0.05 M sodium cacodylate buffer; made up from Electron Microscopy Sciences RT15949, Hatfield,

USA) and incubated for 60 min on a revolver rotator at 4°C. After fixation, cells were washed three times in 1 x phosphate Buffered Saline (PBS, Corning 46-013-CM, Corning, USA) and stored at 4°C for processing. An additional subsample of 100 µl was removed from the tonometers and centrifuged to remove the saline. The RBC pellet was re-suspended in 5 volumes of lysis buffer containing 1 mM DL-Dithiothreitol (DTT; Thermo Fisher R0861; Waltham, USA), 1 mM phenylmethylsulfonyl fluoride (PMSF; Sigma P7626) and 10 mM benzamidine hydrochloride hydrate (BHH; Sigma B6506) in PBS. The RBCs were lysed by three cycles of freeze-thawing in liquid nitrogen, the lysate was centrifuged at 500 *g* for 10 min at 4°C and the supernatant was frozen at -80°C for Western blot processing.

*Hb-$O_2$ binding after β-adrenergic stimulation*

An additional aliquot of RBCs was re-suspended in native plasma at a Hct of 5%. Volumes of 300 µl were loaded into one of four tonometers and equilibrated to arterial gas tensions at 17°C (as described previously) and treated with either: i) a carrier control (DMSO; 0.25%), ii) ISO (10 µM), or iii) ISO+Am (1 mM). These treatments were staggered to allow for standardised measurements at 60 min after drug additions, when 2 µl of blood were removed from the tonometer and loaded into the BOBS for real-time measurements of Hb-$O_2$ saturation during a respiratory acidosis. Therefore, the blood was exposed to stepwise increases in $PCO_2$ (0.3, 0.5, 1, 1.5, 2 and 3%) allowing for two minutes of equilibration at each step; preliminary trials showed full equilibration to the new $PCO_2$ after ~1 min and absorbance remained constant thereafter. As described previously, this protocol also included initial and final calibration steps, at which the sample was fully $O_2$-saturated and then desaturated. A first trial was performed in normoxia (21% $PO_2$) and then a second sample was loaded form the same tonometer for an additional run under hypoxic conditions (3% $PO_2$). The $PO_2$ value in these hypoxic runs was chosen to yield a Hb-$O_2$ saturation close to $P_{50}$ and was informed from the previous measurements of Hb-$O_2$ binding characteristics. Finally, 250 µl of blood were removed from the tonometer for the measurement of blood parameters, as described previously.

*Subcellular localisation of RBC β-NHE*

Fixed RBCs were permeabilized in 1.5 ml 0.1% triton-X100 (VWR Amresco 1421C243) in PBS for 15 min at room temperature on a revolver rotator. Thereafter, the RBCs were blocked for auto-fluorescence in 100 mM glycine in PBS for 15 min, after which the cells were rinsed three times in PBS. For immunocytochemistry, 200 µl of these fixed RBCs were re-suspended in

a blocking buffer containing 3% bovine serum albumin (VWR 0332) and 1% normal goat serum (Lampire Biological Laboratories 7332500; Pipersville, USA) in PBS and incubated for six hours on a rotator. Primary antibodies were added directly into the blocking buffer and incubated on a rotator over-night at 4°C. A monoclonal mouse anti-*Tetrahymena* α-tubulin antibody (deposited by Frankel, J. and Nelsen, E.M at the Developmental Studies Hybridoma Bank, DSHB12G10; Iowa City, USA) was used at 0.24 µg $ml^{-1}$ and a custom, polyclonal, affinity-purified, rabbit anti-rainbow trout β-NHE (epitope: MERRVSVMERRMSH) was used at 0.02 µg $ml^{-1}$. After primary incubations the RBCs were washed three times in PBS and incubated for three hours on a rotator at room temperature in blocking buffer containing secondary antibodies: 1:500 goat anti-mouse (AlexaFlour 568; Thermo Fisher Life Technologies A-11031), 1:500 goat anti-rabbit (AlexaFlour 488; A-11008) and 1:1000 4′,6-diamidino-2-phenylindole (DAPI; Roche 10236276001; Basel, Switzerland). After secondary incubations, RBCs were washed three times and were re-suspended in PBS. To validate the β-NHE antibody, controls were performed by leaving out the primary antibody and by pre-absorbing the primary antibody with its pre-immune-peptide. All images were acquired with a confocal laser-scanning fluorescence microscope (Zeiss Observer Z1 with LSM 800, Oberkochen, Germany) and ZEN blue edition software v.2.6. For super-resolution imaging the cells were re-suspended in PBS with a mounting medium (Thermo Fisher Invitrogen ProLong P36980) and acquisition was with the Zeiss AiryScan detector system. To ensure that images were comparable, the acquisition settings were kept the same between the different treatments and between treatments and the controls. Optical sectioning and three-dimensional (3D) reconstructions of single RBCs from the different treatments were processed with the Imaris software v.9.0. (Oxford Instruments, Abingdon, UK) and rendered into movies.

*Molecular β-NHE characterisation*

For Western blotting, RBC crude homogenates were thawed and centrifuged at 16,000 *g* for one hour at 4°C to obtain a supernatant containing the cytoplasmic fraction and a pellet containing a membrane-enriched fraction that was re-suspended in 100 µl of lysis buffer. The protein concentration of all three fractions was measured with the Bradford's assay (BioRad 5000006; Hercules, USA). Samples were mixed 1:1 with Laemmli's sample buffer (BioRad 161-0737) containing 10% 2-Mercaptoethanol (Sigma M3148) and were heated to 75°C for 15 min. Sample loading was at 5 µg protein from each fraction for the detection of β-NHE and 60 µg

protein from crude homogenate for the detection of α-tubulin, into the lanes of a 5% stacking- and 10% separating polyacrylamide gel. The proteins were separated at 60 V for 30 min and 150 V until the Hb fraction (~16 kDa) ran out the bottom of the gel (~60 min); previous trials had shown that the high Hb content of these lysates may bind some antibodies non-specifically. The proteins were transferred onto a Immun-Blot polyvinylidene difluoride membrane (PVDF; BioRad) using a semi-dry transfer cell (Bio-Rad Trans-Blot SD) over-night, at 90 mA and 4°C. PVDF membranes were blocked over-night, on a shaker at 4°C in tris-buffered saline with 1% tween 20 (TBS-T; VWR Amresco ProPure M147) and 0.1 g $ml^{-1}$ skim milk powder (Kroger; Cincinnati, USA). Primary antibodies were made up in blocking buffer and mixed on a shaker at 4°C, over-night, before applying to the membranes. The anti-α tubulin antibody was used at 4.7 ng $ml^{-1}$, the anti-β-NHE antibody at 0.42 ng $ml^{-1}$ and controls at a peptide concentration exceeding that of primary antibody by 10:1. Primary incubations were for four hours on a shaker at room temperature and membranes were rinsed three times in TBS-T for 5 min. Secondary incubations were with either an anti-rabbit or mouse, horse-radish peroxidase conjugated secondary antibody (BioRad 1706515 and 1706516) for three hours on a shaker at room temperature. Finally, the membranes were rinsed three times in TBS-T for 5 min and the proteins were visualized by enhanced chemiluminescense (BioRad, Clarity 1705061) in a BioRad Universal III Hood with Image Lab software v.6.0.1. Protein sizes were determined relative to a precision dual-colour protein ladder (BioRad 1610374).

The white seabass β-NHE sequence was obtained by transcriptomics analysis of gill samples that were not perfused to remove the blood and these combined gill and RBC tissue samples were stored in RNA later for processing. Approximately 50 µg of sample were transferred into 1 ml of Trizol reagent (Thermo Fisher 15596026) and were homogenized on ice with a handheld motorized mortar and pestle (Kimble Kontes, Dusseldorf, Germany). These crude homogenates were centrifuged at 1000 *g* for 1 min and the supernatant was collected for further processing. RNA was extracted in RNA spin columns (RNAEasy Mini; Qiagen, Hilden, Germany) and treated with DNAse I (ezDNase; Thermo Fisher, 11766051) to remove traces of genomic DNA. RNA quantity was determined by spectrophotometry (Nanodrop 2000; Thermo Fisher) and RNA integrity was determined with an Agilent 2100 Bioanalyzer (Agilent; Santa Clara, USA). Poly-A enriched complementary DNA (cDNA) libraries were constructed using the TruSeq RNA Sample Preparation Kit (Illumina; San Diego, USA). Briefly, mRNA was selected

against total RNA using Oligo(dt) magnetic beads and the retained RNA was chemically sheared into short fragments in a fragmentation buffer, followed by first- and second-stand cDNA synthesis using random hexamer primers. Illumina adaptor primers (Forward P5-Adaptor, 5'AATGATACGGCGACCACCGAGA3'; Reverse P7-Adaptor 5' CGTATGCCGTCTTCTGCTTG 3') were then ligated to the synthesized fragments and subjected to end-repair processing. After agarose gel electrophoresis, 200-300 bp insert fragments were selected and used as templates for downstream PCR amplification and cDNA library preparation. The combined gill and RBC samples (1 µg RNA) were sent for RNAseq Poly-A sequencing with the Illumina NovoSeq™ 6000 platform (Novogene; Beijing, China) and raw reads are made available on NCBI (PRJNA722314).

RNAseq data was used to generate a *de novo* transcriptome assembly which was mined for white seabass isoforms of the Slc9a1 protein family using methods previously described (Clifford et al., 2017). Briefly, raw reads were analysed, trimmed of adaptor sequences, and processed with the OpenGene/fastp software (Chen et al., 2018), to remove reads: i) of low quality (PHRED quality score < 20), ii) containing >50% unqualified bases (base quality < 5), and iii) with >10 unknown bases. Any remaining unpaired reads were discarded from downstream analysis and quality control metrics were carried out before and after trimming (raw reads 80.07 x $10^6$; raw bases 12.01 Gb; clean reads 79.44 x $10^6$, clean bases 11.84 Gb, clean reads Q30 95.26%; GC content 46.67%). Thereafter, fastq files were merged into a single data set, normalized, and used for *de novo* construction of a combined gill and RBC transcriptome using the Trinity v2.6.6 software. Normalization and assembly were performed using the NCGAS (National Centre for Genome Analysis Support) *de novo* transcriptome assembly pipeline (github.com/NCGAS/de-novo-transcriptome-assembly-pipeline/tree/master/Project_Carbonate_v4) on the Carbonate High Performance Computing cluster housed at Indiana University. For assembly, minimum kmer coverage was set to three and the minimum number of reads needed to glue two inchworm contigs together, was set to four (Grabherr et al., 2011). The resulting nucleotide FASTA file was translated into six protein reading frames using BBMap (Bushnell, 2014), which were mined for the NHE-like proteins using HMMER3 v.3.0 (hmmer.org) by querying the *de novo* assembly against a hidden markov model (HHM) homology matrix generated from 132 aligned protein sequences of the vertebrate NHE family (slc9a1 – slc9a9; see Table S1 for accession numbers). Sequences were aligned

using MUSCLE (Edgar, 2004) in SeaView (Galtier et al., 1996; Gouy et al., 2010), with NHE2 from *Caenorhabditis elegans* as an outgroup and results were refined using GBlocks (Castresana, 2000) according to the parameters specified previously (Talavera and Castresana, 2007). Phylogenetic analysis was conducted on the Cyberinfrastructure for Phylogenetic Research (CIPRES) Science Gateway (Miller et al., 2010) using the RAxML software v.8.2.12 (Stamatakis, 2014) with the LG evolutionary and GTRGAMMA models (Le and Gascuel, 2008). Branch support was estimated by bootstraps with 450 replications and the constructed tree was edited in FigTree v.1.4.4. Finally, the open reading frame of the white seabass β-NHE sequence (predicted 747 amino acids), was analysed for the presence of the Kozak nucleic acid motifs (5'-(gcc)gccRccAUGG-3'; Kozak, 1987) immediately upstream of putative start codons, using the ATGpr software (Nishikawa et al., 2000).

To confirm the expression of the β-NHE in the RBCs of white seabass, an additional blood sample of 1 ml was collected and processed as described previously. RBCs were lysed by repeatedly passing them through a 23G needle and RNA extraction was on 50 µg of RBCs by standard Trizol and chloroform extraction following the kit instructions. Isolated RNA was treated with DNAse I and 1 µg RNA was used to synthesize first-strand cDNA using SuperScript IV reverse transcriptase (Thermo Fisher 18090010). Full-length cDNA sequences were obtained in 35 cycles of PCR reactions with Phusion DNA polymerase (New England Biolabs, Ipswich, USA; MO531L) and specific primers designed against the sequence of the phylogenetically characterized white seabass β-NHE obtained from the combined gill and RBC transcriptome (Integrated DNA Technologies, Coralville, Iowa; F: 5'TCC CGT ACT ATC CTC ATC TTC A-3' R: 5'-CCT CTG CTC TCT GAA CTG TAA AT-3'). Amplicons were analysed by gel electrophoresis on a ChemiDoc imaging system (Bio-Rad) that confirmed the presence of a single band (2372 bp**)**. A-overhangs were added to Phusion products with one unit Taq polymerase (New England Biolabs; MO267S) followed by 10 min incubation at 72°C. Products were cloned (TOPO TA Cloning Kit/pCR 2.1-TOPO Vector; Invitrogen; K4500) and the ligated product was transformed into TOP10 chemically competent *E. coli* cells (Invitrogen; K457501) according to manufacturer specifications. Following over-night incubation at 37°C, single colonies of transformants were grown in Luria-Bertani (LB) broth over-night on a shaking incubator (37°C, 220 rpm; Barnstead MaxQ 4000). Plasmid DNA was isolated (PureLink Quick

Plasmid Miniprep kit; Invitrogen K210010) according to manufacturer specifications and inserts were sequenced to confirm their identity and uploaded to NCBI (MW962257).

*Calculations and statistical analysis*

All data were analysed with R v.4.0.4 (RCoreTeam, 2020) in RStudio v.1.4.1106 (RStudioTeam, 2021) and figures were created with the ggplot2 package (Wickham, 2009). Normality of the residuals was tested with the Shapiro-Wilk test (stat.desc function in R) and homogeneity of variances was confirmed with the Levene's test (leveneTest function in R). Deviations from these parametric assumptions were corrected by transforming the raw data.

To determine the blood $O_2$-binding characteristics, Hb $P_{50}$ and $n_H$ values were those determined with the BOBS software v.1.0.20 (Loligo) and oxygen equilibrium curves (OEC) were generated by fitting a two parameter Hill function to the mean $P_{50}$ and $n_H$ for 8 individual fish. The main effects of $PCO_2$ on $P_{50}$ and $n_H$ were analysed with ACOVA ($P < 0.05$, $N = 8$). Plasma [$HCO_3^-$] was calculated from $TCO_2$ by subtracting the molar [$CO_2$] calculated from the dissociation constant and solubility coefficients in plasma at 17°C and the corresponding sample pH (Boutilier et al., 1984). The Bohr effects relative to $pH_i$ and $pH_e$, the relationship between RBC $pH_i$ and $pH_e$ and the non-bicarbonate buffer capacity of whole blood were determined by linear regression analysis, results of which are shown in detail in the supplement (Fig. S1A-D). The average values for these blood characteristics are shown in the main text and were calculated as the average slopes across all individuals.

In the RBC swelling trial, mean cell Hb was calculated as [Hb] divided by Hct as a decimal. Since Hb is a membrane impermeable solute, MCHC is used as a common indicator of RBC swelling. Main effects of drugs (DMSO, ISO and ISO+Am), time (10, 30 and 60 min) and their interaction (drug×time) on Hct, [Hb], MCHC, $pH_e$ and $pH_i$ were determined by two-way ANOVAs (lm and Anova functions in R; $N = 5$-6; $P < 0.05$) and multiple comparisons were conducted with t-tests (pairwise.t.test function in R) and controlling the false detection likelihood (FDR) with a Benjamini-Hochberg correction (p.adjust function in R).

The effect of RBC β-adrenergic stimulation on Hb-$O_2$ binding was assessed by analysing the absorbance data from the BOBS with a custom R script (github.com/tillharter/White-Seabass-beta-NHE). In brief, the absorbances recorded at 430 nm were divided by the isosbestic wavelength of 390 nm (where absorbance is independent of Hb-$O_2$ binding), and these ratios were used as the raw data for subsequent analyses. For each trace, the ten final absorbance ratios

at each equilibration step were averaged (i.e. 10 s) and Hb-$O_2$ saturation was calculated relative to the absorbance at the two initial calibration conditions (i.e. high: 99.7% $PO_2$, 0.3% $PCO_2$; and low 0% $PO_2$, 0.3% $PCO_2$), assuming full saturation or desaturation of Hb, respectively. These calibration values were measured again at the end of each trial and a linear correction of drift was performed for each sample. The resulting values for Hb-$O_2$ saturation were plotted against $PCO_2$ and several non-linear models were fit to the data (Michaelis-Menten, Exponential and Hill). The model with the best fit (lowest AIC) was a three-parameter Hill function that was applied to each individual trace. The parameter estimates from this model yielded the maximal reduction in Hb-$O_2$ saturation (Max. $\Delta$Hb-$O_2$ sat.; %) and the $PCO_2$ at which this response was half-maximal ($EC_{50}PCO_2$; %). The main effects of drugs (DMSO, ISO and ISO+Am), $O_2$ (normoxia and hypoxia) and their interaction (drug×$O_2$) on the parameter estimates from the Hill functions were determined by two-way ANOVAs (lm and Anova functions in R; $N = 6$; $P < 0.05$). When significant main effects were detected, multiple comparisons were conducted with t-tests (pairwise.t.test function in R) and controlling the false detection likelihood (FDR) with a Benjamini-Hochberg correction (p.adjust function in R). The Root effect was determined as the Max. $\Delta$Hb-$O_2$ sat. of the control treatment (DMSO). To quantify the relative changes in Hb-$O_2$ saturation ($\Delta$Hb-$O_2$ sat.) due to drug treatments, data were expressed relative to the paired measurements in the DMSO treatment for each individual fish and relative to the initial Hb-$O_2$ saturation at 0.3% $PCO_2$ (i.e. 95.6 and 55.0% Hb-$O_2$ saturation in normoxia and hypoxia, respectively). All data are presented as means±s.e.m.

## Results

### *Blood $O_2$-binding characteristics*

The blood $O_2$-binding characteristics of white seabass are summarised in Figure 1. When $PCO_2$ was increased from arterial tension (0.3%) to severe hypercapnia (2.5%) Hb $P_{50}$ increased significantly from 21.4±0.5 to 88.6±2.6 mmHg. At the same time, the cooperativity of Hb-$O_2$ binding, expressed by $n_H$, decreased significantly from 1.52±0.04 to 0.84±0.03, which was reflected in a change in shape of the OECs from sigmoidal to hyperbolic. Over the tested range of $PCO_2$, white seabass displayed a Bohr coefficient of -0.92±0.13 when expressed relative to the change in $pH_e$ and -1.13±0.11 when expressed relative to the change in RBC $pH_i$ (Fig. S1A and B). In addition to the reduction in Hb-$O_2$ affinity at elevated $PCO_2$, white seabass blood also displayed a large Root effect with a maximal reduction of Hb-$O_2$ carrying capacity of 52.4±1.8%. The relationship between $pH_i$ and $pH_e$ had a slope of 0.67±0.07 (Fig. S1C), reflecting the higher buffer capacity of the intracellular space. The non-bicarbonate buffer capacity of white seabass whole blood was -2.43±0.56 mmol $l^{-1}$ $pH_e^{-1}$ at a Hct of 5% (Fig. S1D). By correcting this value for the higher Hct *in vivo*, according to Wood et al. (1982), white seabass with a Hct of 25% are expected to have a whole blood non-bicarbonate buffer capacity of -9.68 mmol $l^{-1}$ $pH_e^{-1}$.

### *RBC swelling after β-adrenergic stimulation*

The β-adrenergic stimulation of white seabass blood with ISO induced changes in the measured blood parameters (Fig. 2). Significant main effects of drug, time and their interaction (drug×time), indicate that Hct was affected by the experimental treatments (Fig. 2A). A large increase in Hct was observed in ISO-treated blood that was absent in ISO+Am and DMSO-treated RBCs. In addition, a main effect of drug treatment on MCHC indicated that the increase in Hct after ISO addition was due to swelling of the RBCs, whereas [Hb] was not affected by the treatments (Fig. 2B). Significant main effects of drug and time were also detected for $pH_e$, where a large extracellular acidification was observed in ISO-treated blood, relative to the DMSO and ISO+Am treatments (Fig. 2C). No significant main effect of drug or time were observed on RBC $pH_i$, but multiple comparisons indicated a trend for a higher $pH_i$ in ISO compared to DMSO treated blood ($P$ = 0.081; Fig. 2D). Differential interference contrast (DIC) images confirmed a normal morphology of the RBCs at the beginning and the end of the trials, thus validating the fixation procedure. Swelling was observed in ISO-treated RBCs, relative to initial measurements

or DMSO and ISO+Am-treated cells (Fig. 2E-H). The swelling of ISO-treated RBCs occurred largely along the z-axis of the cells (indicated by the arrows), whereas no visible distortion was observed in the x-y directions.

*Molecular β-NHE characterisation*

The combined gill and RBC *de novo* transcriptome of white seabass contained nine Slc9a1 transcripts and phylogenetic analysis placed these sequences within well-supported clades of the NHE family tree (Fig. 3). Importantly, one of these white seabass transcripts grouped with the Slc9a1b sequences from other teleost fishes, supporting its classification as a white seabass β-NHE. Results from RT-PCR, cloning and sequencing confirmed the expression of β-NHE mRNA in isolated white seabass RBCs. A search for the Kozak nucleic acid motif in the open reading frame of the white seabass β-NHE sequence yielded the five most likely potential start codons, including one that would produce a 66 kDa protein (Table S2). This size closely matched the single band that was specifically recognized by the polyclonal β-NHE antibody in Western blots with crude homogenate, cytosolic and membrane-enriched fractions of a white seabass RBC lysate (Fig. S2A); whereas no immunoreactivity was observed in lanes where the antibody had been incubated with its pre-immune peptide. The anti-α-tubulin antibody detected a single band in the RBC crude homogenate, at the predicted size of 54 kDa (Fig. S2B). Finally, the white seabass β-NHE protein sequence shared seven consecutive amino acids with the peptide used to raise the polyclonal antibodies (Fig. S2C), which is sufficient for specific antibody binding (Dunn et al., 1999). More importantly, the antigen peptide sequence was absent in the other eight white seabass NHE isoforms, ruling out non-specific antibody recognition of these NHEs.

*Subcellular localisation of RBC β-NHE*

The subcellular location of β-NHE protein in white seabass RBCs was determined by immunofluorescence cytochemistry and super-resolution confocal microscopy (Fig. 4). In DMSO-treated RBCs, the β-NHE immunolabelling was most intense in intracellular vesicle-like structures, and weaker at the plasma membrane. There was substantial heterogeneity in the staining pattern for β-NHE in these control cells, with varying amounts of intracellular and membrane staining. In ISO-treated RBCs, the staining pattern for β-NHE was more homogeneous and most cells showed intense immunoreactivity for β-NHE in the membrane that co-localised with α-tubulin in the marginal band, and the intracellular, vesicle-like staining that

was observed in the control cells was reduced (see Fig. S3 for an overview image with more cells). In contrast, ISO-treated cells that were incubated without the primary antibody or where the antibody was pre-absorbed with its pre-immune-peptide showed no immunoreactivity for β-NHE (Fig. S4). Finally, optical sectioning and three-dimensional reconstruction of these RBCs confirmed that the membrane staining for β-NHE occurred in a single plane and co-localised with α-tubulin in the marginal band (see 3D Movies S1 and S2).

*Hb-$O_2$ binding after β-adrenergic stimulation*

To study whether the activation of RBC β-NHEs in white seabass has a protective effect on Hb-$O_2$ binding, blood samples were first equilibrated to 21% $PO_2$ and 0.3% $PCO_2$ in tonometers and no significant effects of drug treatment (DMSO, ISO or ISO+Am) were observed on any of the measured blood parameters and average values were: Hct 5.20±0.14% ($P$ = 0.095), [Hb] 0.178±0.006 mM ($P$ =0.889), MCHC 3.46±0.15 mM $L^{-1}$ RBC ($P$ = 0.490), $pH_e$ 7.848±0.018 ($P$ = 0.576), $pH_i$ 7.464±0.021 ($P$ = 0.241). Thereafter, blood was loaded into the BOBS, where Hb-$O_2$ saturation was measured spectrophotometrically at increasing levels of a respiratory acidosis in normoxia (21% $PO_2$). As expected from the pH-sensitivity of Hb-$O_2$ binding in white seabass, an increase in $PCO_2$ from 0.3 to 3% caused a severe reduction in Hb-$O_2$ saturation in all treatments via the Root effect (Fig. 5). The raw data were analysed by fitting a three-parameter Hill model to the individual observations within each treatment and significant differences were observed in the parameter estimates that describe these models. $EC_{50}PCO_2$ was affected by the experimental treatments, as shown in a significant main effect of drug (Fig. 6A). Multiple comparisons confirmed significant differences in $EC_{50}PCO_2$, which was 0.85±0.06% in DMSO, 0.91±0.06% in ISO+Am and 1.08±0.06% in ISO-stimulated blood. In contrast, the magnitude of the responses, Max. ΔHb-$O_2$ sat., was not affected by the experimental treatments and no significant main effect of drug was detected; the average Max. ΔHb-$O_2$ sat. across treatments was -51.1±0.7% (Fig. 6B).

When the same experiment was repeated under hypoxic conditions (3% $PO_2$), an increase in $PCO_2$ likewise caused a severe reduction in Hb-$O_2$ saturation, indicating that in white seabass, a Root effect can also be expressed at saturations around $P_{50}$ (Fig. 5). A significant main effect of $O_2$ indicated that cells in the hypoxic condition required a lower $EC_{50}PCO_2$ to achieve Max. ΔHb-$O_2$ sat., compared to the normoxic condition (Fig. 6A). There was also a significant main effect of drug on $EC_{50}PCO_2$ and multiple comparisons indicated a similar pattern in the

514 individual drug effects as in the normoxic experiment, which was further confirmed by the
515 absence of a significant drug×$O_2$ interaction. Finally, a significant effect of $O_2$ on Max. $\Delta$Hb-$O_2$
516 sat. (Fig. 6B) indicated a larger response magnitude in hypoxic blood, but that was unaffected by
517 drug treatments, and the average Max. $\Delta$Hb-$O_2$ sat. across treatments was -74.1±0.1%.
518 To quantify the benefit of β-adrenergic stimulation during a hypercapnic acidosis, Hb-$O_2$
519 saturation was expressed relative to the paired measurements in the DMSO treatment for each
520 individual fish and relative to the initial Hb-$O_2$ saturation at 0.3% $PCO_2$ (i.e. 95.6 and 55.0% Hb-
521 $O_2$ saturation in normoxia and hypoxia, respectively). In normoxia, the benefit of β-NHE
522 stimulation with ISO showed a bell-shaped relationship with a maximal $\Delta$Hb-$O_2$ sat. of
523 7.8±0.02% at 1% $PCO_2$ (Fig. 7A). When NHEs were inhibited in ISO+Am blood, $\Delta$Hb-$O_2$ sat.
524 was only 1.9±0.4% at 1% $PCO_2$ and significantly lower compared to the other treatments; at
525 higher $PCO_2$ the 95% confidence intervals overlapped with the DMSO values, indicating no
526 difference from controls. In hypoxic blood, the ISO treatment had the largest effects on $\Delta$Hb-$O_2$
527 sat. at 0.3% $PCO_2$, with maximal values of 19.2±0.0% that decreased towards higher $PCO_2$ (Fig.
528 7B). Whereas, in the ISO+Am treatment, $\Delta$Hb-$O_2$ sat. was 6.4±0.0% at 0.3% $PCO_2$, and
529 significant differences to the DMSO controls were only observed at $PCO_2$ below 1.5%.

## Discussion

In line with our initial hypothesis, white seabass RBCs had β-NHE activity that protected the blood $O_2$-carrying capacity during hypoxic and hypercapnic conditions. However, not all predictions were met as expected: white seabass did not have an unusually high Hb-$O_2$ affinity and thus, other aspects of their physiology are likely more important in determining their tolerance to hypoxia. Like other teleosts, white seabass had highly pH-sensitive Hbs, where a reduction in pH decreased both Hb-$O_2$ affinity via the Bohr effect and Hb-$O_2$ carrying capacity via the Root effect. Several lines of evidence corroborated the presence of a RBC β-NHE in white seabass and super-resolution imaging revealed, for the first time, the subcellular location of β-NHE protein in intracellular vesicles and on the RBC membrane. Furthermore, adrenergic stimulation induced changes in the intracellular distribution of the β-NHE that may indicate a role of protein translocation in regulating β-NHE activity. The activation of RBC β-NHEs significantly increased Hb-$O_2$ saturation during *in-vivo* relevant conditions of hypercapnic acidification. In fact, the largest benefit of β-NHE activation in normoxia was observed at ~1% $PCO_2$, where Hb-$O_2$ saturation increased by ~8%. Whereas in hypoxia (3% $PO_2$), β-NHE activity had its largest effect at arterial $PCO_2$ (0.3%) and enhanced Hb-$O_2$ saturation by ~20%. However, the benefits of β-NHE activation in hypoxia decrease rapidly at higher $PCO_2$, revealing a potential vulnerability of white seabass to combinations of these stressors.

Many hypoxia tolerant vertebrates have evolved Hbs with a high affinity for $O_2$ (low Hb $P_{50}$ values), which helps them extract the gas from the respiratory medium (Hughes, 1973; Mairbäurl, 1994; Tenney, 1995). White seabass in the present study had a Hb $P_{50}$ of 21.4±0.5 mmHg (Fig.1), which is higher than the values typically found in hypoxia tolerant fishes, such carp (*Cyprinus carpio*) that have Hb $P_{50}$ values as low as 3.6 mmHg (Brauner et al., 2001). In fact, the Hb $P_{50}$ of white seabass resemble more closely the values in the well-studied rainbow trout, of 24.8 mmHg (Rummer and Brauner, 2015), a cold-stream salmonid, of no noteworthy hypoxia tolerance. However, the $O_2$-binding affinity of Hb is a trade-off that must strike a balance between loading $O_2$ at the gas exchange surface and unloading $O_2$ at the tissues (Brauner and Wang, 1997). Everything else being equal, a higher Hb $P_{50}$ can sustain a higher $PO_2$ at the tissue capillaries, enhancing the diffusion gradient of $O_2$ to the mitochondria, which is of particular benefit to those species with a high scope for exercise (Mairbäurl and Weber, 2012). Thus, it seems that a high Hb-$O_2$ affinity is not part of the physiological mechanism that

facilitates hypoxia tolerance in white seabass, but instead, a high tissue $PO_2$ may be important to sustain exercise performance in these active piscivours.

As in other teleosts, especially those in the highly-derived group of perciformes, Hb-$O_2$ binding in white seabass was highly pH-sensitive. An increase in $PCO_2$ from arterial levels (0.3%) to severe hypercapnia (2.5%), caused a significant right-shift of the OEC (Fig. 1) via the Bohr effect, increasing $P_{50}$ to 88.6±2.6 mmHg. When considering the corresponding changes in $pH_e$ (from 8.1 to 7.2 over the range of tested $PCO_2$; see Fig. S1A) the Bohr coefficient in white seabass was -0.92, and slightly higher, at -1.13, when considering the changes in RBC $pH_i$ (from 7.7 to 7.0: Fig. S1B). Again, these Hb-$O_2$ binding characteristics resemble closely those of rainbow trout, where $P_{50}$ increases to 75 mmHg at 2% $PCO_2$, yielding a Bohr coefficient (relative to $pH_e$) of -0.87 (Rummer and Brauner, 2015). A normoxic increase in $PCO_2$ caused a significant reduction in Hb-$O_2$ saturation via the Root effect, and at $PCO_2$ above 3% the $O_2$-carrying capacity of white seabass Hb was reduced by 52.4±1.8%. These results are in line with those of other teleosts, such as rainbow trout (~55%), tench (*Tinca tinca*; ~50%) and the European perch (*Perca fluviatilis*; ~70%), where the larger Root effect values may reflect the higher final $PCO_2$ used during those trials (Berenbrink et al., 2011).

The Root effect is part of a specialized system of $O_2$ supply to the eye and the swimbladder of teleosts, where blood is acidified in a counter-current exchanger (the *rete mirabile*) to produce high $PO_2$ that bridge the large diffusion distances to the avascular retina of teleosts and inflate the swimbladder against large hydrostatic pressures (Pelster and Randall, 1998). In the course of teleost evolution there have been numerous secondary losses of the *choroid* and swimbladder *retes*. While their presence has not directly been determined in white seabass, an ancestral state reconstruction predicts no secondary loss of either *rete* on the teleost branch leading up to the perciformes, which include the white seabass (Berenbrink et al., 2005). In addition, all of the five independent losses of the *choroid rete* have coincided with a reduction of the Root effect below 40% (Berenbrink, 2007; Berenbrink et al., 2005). Thus, the large Root effect of white seabass is consistent with the presence of a *choroid rete* and likely critical for maintaining a high ocular $PO_2$ that facilitates the visual acuity in these active predators (Damsgaard et al., 2020).

Vertebrate Hbs are intracellular proteins and, as such, are affected by the microenvironment within the RBC cytoplasm. Teleost β-NHEs can actively modulate Hb-$O_2$

592 binding by controlling RBC $pH_i$ and several lines of evidence in our study indicate the presence
593 of functional β-NHEs in white seabass RBCs. A combined gill and RBC transcriptome detected
594 nine sequences belonging to the vertebrate NHE (Slc9a1) family and phylogenetic analysis
595 classified the white seabass Slc9a1b transcript as belonging to the larger group of teleost RBC β-
596 NHEs (Fig. 3). These findings were supported by the results from RT-PCR confirming the
597 expression of the β-NHE in white seabass RBCs. Western blots with a polyclonal anti-trout β-
598 NHE antibody recognized a single band at 66 kDa in white seabass RBC homogenates (Fig.
599 S2A), which is smaller than the 84 kDa predicted based on the longest possible mRNA transcript
600 (Table S2). However, a search for Kozak motifs revealed the five most likely potential start
601 codons in the open reading frame of the white seabass β-NHE mRNA sequence, one of which
602 predicted a protein size of 66 kDa that matches the protein size detected in Western blots. This
603 predicted β-NHE isoform lacks 158 amino acids on the N-terminus, which, according to
604 structural models for NHE proteins (Landau et al., 2007), are not essential for the transporter's
605 activity, but may determine a differential sensitivity to inhibitors (Landau et al., 2007; Lee et al.,
606 2011). NHE isoforms from other teleosts have been shown to separate in Western blotting with a
607 similar size discrepancy (Chen et al., 2017), and also show differential sensitivity to amiloride
608 and its derivatives compared to mammalian NHEs (Blair et al., 2021).
609 Adrenergic stimulation of white seabass RBCs with ISO caused a ~25% volume increase
610 in the course of 60 min, whereas no changes in RBC volume were detected in DMSO treated
611 cells. The swelling response was corroborated by a significant reduction in MCHC and by
612 visually confirming the increase in cell volume under a microscope; these results closely match
613 previous reports of RBC swelling after adrenergic stimulation in other teleosts (Nikinmaa and
614 Huestis, 1984; Shu et al., 2017; Weaver et al., 1999). In addition, the ISO-induced swelling was
615 completely abolished by the inhibition of NHEs in ISO+Am-treated RBCs, providing additional
616 pharmacological support for the presence of a RBC β-NHE in white seabass. In ISO-treated
617 RBCs, but not those treated with DMSO or ISO+Am, we observed a decrease in $pH_e$, which is
618 the direct result of $H^+$ excretion by NHE activity. Corresponding changes in RBC $pH_i$ are
619 typically smaller, due to the higher buffer capacity of the intracellular space ($pH_i$ =
620 $0.67\pm0.07\times pH_e$; Fig. 1) and the freeze-thaw method is typically associated with a larger error
621 compared to $pH_e$ measurements. Consequently, we were not able to resolve significant treatment
622 effects on RBC $pH_i$, but a non-significant trend may point towards a small increase in RBC $pH_i$.

Another interesting observation in these RBC swelling trials were the changes in cell morphology due to adrenergic stimulation. The increase in cell volume was largely due to an expansion along the z-axis of the cells, whereas the dimensions in the x-y axis apparently remained unaffected. The nucleated RBCs of non-mammalian vertebrates, including fish, have a marginal band, a structural component of their cytoskeleton formed by strands of α-tubulin that maintains their elliptical shape in the face of shear and osmotic disturbances (Joseph-Silverstein and Cohen, 1984). The stiffness of this marginal band (Dmitrieff et al., 2017) may be a major impediment to swelling along the x-y axis forcing the cells to widen in the z-direction.

Fixed RBCs from these swelling trials were studied in more detail by super-resolution microscopy and by immunolabelling β-NHE and α-tubulin (Fig. 4). All RBCs showed β-NHE immunoreactivity, corroborating the presence of β-NHE protein in these cells. In control RBCs, β-NHE protein was detected intracellularly and appeared to be confined to vesicles, while weaker staining was detected on the plasma membrane (Fig. 4C, D and S3). A similar staining pattern has been described for a NHE1-like protein in the RBCs of winter flounder (*Pseudopleuronectes americanus*; Pedersen et al., 2003). However, the immunolabelling of this NHE was with polyclonal antibodies raised against a region of the human NHE1 sequence (aa 631-746) that is highly conserved with both the teleost Slc9a1a and Slc9a1b isoforms. Therefore, these previous results likely include staining of several NHE isoforms including the flounder β-NHE. The antibody used in the present study showed a high specificity for the white seabass β-NHE (Fig. S2) and a confounding detection of other RBC NHE isoforms is unlikely.

Strikingly, the intracellular localization of β-NHE protein changed after incubating RBCs with ISO for 60 min. In these stimulated RBCs the staining pattern for β-NHE was more homogeneous compared to controls, with strong signal at the plasma membrane, and weaker intracellular signal (Fig. 4G, H and S3). Optical sectioning and 3D reconstructions of these cells clearly showed that the intense membrane staining for β-NHE was confined to a single plane, colocalizing with α-tubulin in the marginal band, and that this staining was mostly absent in DMSO-treated cells (Movies S1 and S2). Furthermore, the use of super-resolution microscopy allowed us to discern the subcellular orientation the β-NHE signal, which was extracellular relative to α-tubulin (Fig. 4H), thus, indicating a direct contact with the blood plasma that is essential for regulating $pH_i$ via NHE activity. Combined, these observations may point towards an adrenergically-induced translocation of β-NHE protein from the cytoplasm into the membrane

of white seabass RBCs. Intracellular translocation of NHEs in response to various stimuli has been reported in other systems, such as the gills of acid infused hagfish (Parks et al., 2007), insulin-treated rat cardiomyocytes (Lawrence et al., 2010), isolated mammalian cells after acidification (Gens et al., 2007) or the initiation of $Na^+$-glucose co-transport in intestinal epithelial cells (Zhao et al., 2004). Our results may indicate the presence of a similar mechanism for the teleost RBC β-NHE, where further research is needed to quantify the translocation of β-NHE protein, resolve its time-course, and characterise the underlying cellular mechanisms. If substantiated, these findings may open new avenues in the research of RBC $pH_i$ regulation in teleosts and perhaps other vertebrates.

The activation of RBC β-NHEs has been shown to raise $pH_i$ above the equilibrium condition and plays an important role in protecting Hb-$O_2$ binding in teleosts (Nikinmaa, 1992). Previous work has characterised the resulting left-shift in the OEC (Jensen et al., 1983; Nikinmaa, 1983; Nikinmaa and Soivio, 1979) and the changes in arterial $O_2$-carrying capacity due to adrenergic stimulation of the RBCs (Cossins and Richardson, 1985; Ferguson et al., 1989; Nikinmaa et al., 1984). In the present study we quantified the protective effect of β-NHE activation on Hb-$O_2$ saturation in white seabass under environmentally relevant levels of hypercapnia and hypoxia. As expected, Hb-$O_2$ saturation decreased significantly, due to the Root effect, when $PCO_2$ was increased from 0.3-3% (Fig. 5). Adrenergic stimulation of the RBCs with ISO significantly delayed the reduction in Hb-$O_2$ saturation to higher $EC_{50}PCO_2$ that were 1.08±0.06% in ISO compared to 0.85±0.06% in DMSO-treated blood (Fig. 6A). In ISO+Am-treated RBC, the $EC_{50}PCO_2$ decreased significantly to 0.91±0.06%, compared to ISO-treated cells, corroborating the involvement of the RBC β-NHE in the response. However, the $EC_{50}PCO_2$ of ISO+Am-treated RBCs was still significantly higher compared to DMSO controls, perhaps indicating that 1 mM amiloride did not lead to a full inhibition of the β-NHE under the tested conditions, or that other, amiloride insensitive transporters, play a role in elevating RBC $pH_i$ after adrenergic stimulation.

While β-NHE activity shifted the reduction in Hb-$O_2$ saturation to a higher $PCO_2$, the magnitude of the Root effect was not affected by adrenergic stimulation (Fig. 6B). No significant differences were observed in Max. $\Delta$Hb-$O_2$ sat. in any of the tested treatments and therefore, a severe acidosis generated by high $PCO_2$ can overwhelm the physiological capacity of the β-NHE to maintain an elevated RBC $pH_i$. The $H^+$ extrusion by the β-NHE is secondarily active and

driven by the trans-membrane $Na^+$ gradient created by the RBC $Na^+$-$K^+$-ATPase (NKA). While both NKA activity (Bourne and Cossins, 1982) and the RBC rate of $O_2$ consumption ($\dot{M}O_2$) increase after adrenergic stimulation (Boutilier and Ferguson, 1989), it is possible that the capacity of the NKA to maintain the larger $Na^+$ gradients required to compensate for a greater reduction in $pH_i$ is limited, as could be the availability of ATP to fuel the exchange. In addition, $H^+$ that are extruded by the β-NHE will react with $HCO_3^-$ in the plasma to form $CO_2$ that can, once again, diffuse into the cells. This re-acidification of the cells via $CO_2$ is part of the Jacobs-Stewart cycle and typically rate-limited by the formation of $CO_2$ in the plasma of teleosts (Jacobs and Stewart, 1942). However, as $pH_e$ decreases, the pool of plasma $H_2CO_3$ becomes larger (Motais et al., 1989), accelerating the Jacobs-Stewart cycle and the re-acidification of the cells, which may explain, in part, why β-NHE activity is ineffective at very high $PCO_2$.

The benefit of β-NHE activity on Hb-$O_2$ saturation was non-linear over the range of $PCO_2$ tested, and in normoxia the bell-shaped response had a maximum at ~1% $PCO_2$ (Fig. 7A). The observed relationship is likely dependent on the sigmoidal shape of the OEC, where a left-shift due to β-NHE activity has only marginal effects when Hb-$O_2$ saturation is high and the curve is flat (Kobayashi et al., 1994). In addition, β-NHE activity in many teleosts is stimulated by high intracellular [$H^+$] and inhibited by higher extracellular [$H^+$] as $pH_e$ decreases, yielding a bell-shaped relationship between β-NHE activity and pH (Borgese et al., 1987). The ecological implications are noteworthy, as the protective effect of β-NHE activity on Hb-$O_2$ binding is greatest over the range of $PCO_2$ that white seabass are currently experiencing during severe red-tide or upwelling events. The increase in Hb-$O_2$ saturation at these $PCO_2$ is ~8%, and the effect can be harnessed continuously with every pass of the RBCs through the gills. Everything else being equal, an increase in arterial $O_2$ content can sustain a proportionally higher $\dot{M}O_2$, increasing the scope for activity or reducing the requirements for anaerobic pathways of ATP production that can lead to a toxic accumulation of metabolic by-products, such as lactate and $H^+$. Thus, for fish that experience a potentially life-threatening surge in $PCO_2$, an 8% increase in arterial $O_2$ content could make the difference between escaping into less-noxious waters or perishing in the attempt.

In the hypoxic trials, DMSO treated blood at arterial $PCO_2$ (0.3%) had a Hb-$O_2$ saturation of 55.0±3.3%, which was close to the target value around Hb $P_{50}$ (Fig. 5). As in normoxia, an increase in $PCO_2$ caused a significant reduction in Hb-$O_2$ saturation, indicating the presence of a

Root effect in hypoxia, which further decreased Hb-$O_2$ saturation, even below the level of the maximal normoxic Root effect. Consequently, $H^+$ binding to Hb must occur over nearly the entire range of the OEC, which stands in contrast to previous findings in rainbow trout where the Bohr effect and $H^+$ binding to Hb occurred largely in the upper half of the OEC (Brauner et al., 1996; Brauner et al., 2000b). The possibility of inter-specific differences in the interaction between Hb-$O_2$ and $H^+$ binding cannot be resolved from the present data. However, it seems more likely that the kinetics of $H^+$ binding that induce the Bohr effect are different from those of the Root effect, which is supported by previous work indicating different molecular mechanisms for the two effects (Brittain, 1987; Perutz and Brunori, 1982). The interacting kinetics of $O_2$ and $H^+$ binding to the Root effect Hbs of teleosts remain a worthwhile avenue for future research and studying a broader range of environmental and metabolic scenarios, in more species, may strengthen the important ecological implications of the present work.

As in normoxic blood, adrenergic activation of the β-NHE in hypoxia, increased Hb-$O_2$ saturation during a hypercapnic acidosis. This protective effect of the β-NHE was reflected in a significantly higher $EC_{50}PCO_2$ in ISO- compared to DMSO or ISO+Am-treated RBCs (Fig. 6A). A significant main effect of $O_2$ on $EC_{50}PCO_2$, would indicate that in hypoxic blood a lower $PCO_2$ is required to desaturate Hb, compared to normoxic blood. However, this parameter estimate is influenced by the combined effects of $PO_2$ and $PCO_2$ on Hb-$O_2$ saturation (by taking into account the full scale from 0-100%), which is not easily untangled statistically. Importantly, there was no drug×$O_2$ interaction, indicating that the effect of the drugs was similar under normoxia and hypoxia, highlighting the benefit of β-NHE activation under both conditions.

In hypoxia, the benefit of β-NHE activation on Hb-$O_2$ saturation was also non-linear over the tested range of $PCO_2$ (Fig. 7B). β-NHE activation in hypoxic blood caused the largest increase in Hb-$O_2$ saturation at arterial $PCO_2$ (0.3%) and the benefits decreased markedly towards higher levels of hypercapnia; likely due to the flattening of the OEC at low Hb-$O_2$ saturations and perhaps some inhibition of the transporter by the increasing extracellular [$H^+$]. In hypoxic blood, β-NHE activity had a larger effect on Hb-$O_2$ binding compared to normoxic blood, and at 0.3% $PCO_2$, increased Hb-$O_2$ saturation by 11±0.4%. This effect is even greater when considering that the available $O_2$-carrying capacity is lower in hypoxia and when expressed relative to the available Hb-$O_2$ saturation (55% in DMSO treated blood), the relative benefit of β-NHE activity was 19.2±0.0%. Many teleost β-NHEs are $O_2$-sensitive (Gibson et al., 2000) and

747 the larger effects of β-NHE activity on Hb-$O_2$ saturation in hypoxia may be related to a partial
748 inhibition of the transporter in normoxia; whereas, the effect appears to be less severe in white
749 seabass compared to other species (Motais et al., 1987; Salama and Nikinmaa, 1988; Weaver et
750 al., 1999). The nearly 20% increase in Hb-$O_2$ saturation due to β-NHE activity is of great
751 ecological significance and could be a principal pathway to safeguard arterial $O_2$ transport and
752 facilitate the hypoxia tolerance of white seabass in the wild. However, the present data also
753 indicate a diminishing benefit of the β-NHE response when $PCO_2$ increases; thus, revealing a
754 potential vulnerability of white seabass to the combined stressors of hypoxia and hypercapnia;
755 surviving these conditions likely requires additional behavioural and metabolic adjustments, that
756 are yet to be determined.

## Conclusion

The present results provide a thorough characterisation of the Hb-$O_2$ binding system of white seabass, a non-model marine teleost with great ecological and economic importance in Southern California. Several lines of evidence confirmed the presence of a RBC β-NHE and super-resolution microscopy may point towards the regulation of the transporter's activity via intracellular translocation, a potentially novel pathway that deserves a more thorough investigation. In white seabass, the activity of the RBC β-NHE provides significant protection of Hb-$O_2$ binding during hypercapnic conditions with maximal benefits around the ecologically relevant level of ~1% $PCO_2$. Large benefits of β-NHE activation were also observed in hypoxia, however, with a greater sensitivity to increases in $PCO_2$. Combined, these data indicate that RBC function plays a critical role in modulating the $O_2$-binding characteristics of the pH-sensitive Hbs in white seabass and is likely part of the suite of physiological responses that determines their hypoxia and hypercapnia tolerance. Finally, these results also highlight a potential vulnerability of white seabass to combinations of these stressors and further research is needed to study the implications for wild fish conservation along the steadily warming and eutrophicated Californian coast and in high density aquaculture.

773 **Acknowledgements**

774 Thanks are due to Mark Drawbridge at the Hubbs SeaWorld Research Institute (HSWRI)
775 for generously providing the white seabass and Phil Zerofski, Jessica Hallisey, Garfield Kwan
776 and Daniel Jio for their help with animal care.

## Competing interests

The authors declare no competing interests.

779 **Funding**

780 The present study was funded by a National Science Foundation (NSF) grant to MT

781 (award no. 1754994) and AMC was supported by a SIO Postdoctoral Scholar fellowship.

## Data Availability

All data are made available through github (github.com/tillharter/White-Seabass-beta-NHE) for R source codes and raw data files and NCBI for sequence data (see detailed accession numbers in manuscript and supplement).

## References

**Berenbrink, M.** (2007). Historical reconstructions of evolving physiological complexity: $O_2$ secretion in the eye and swimbladder of fishes. *J. Exp. Biol.* **210**, 1641–1652.

**Berenbrink, M., Koldkjaer, P., Kepp, O. and Cossins, A. R.** (2005). Evolution of oxygen secretion in fishes and the emergence of a complex physiological system. *Science* **307**, 1752–1757.

**Berenbrink, M., Koldkjaer, P., Wright, E. H., Kepp, O. and da Silva, A. J.** (2011). Magnitude of the Root effect in red blood cells and haemoglobin solutions of fishes: a tribute to August Krogh. *Acta Physiol.* **202**, 583–592.

**Blair, S., Li, X., Dutta, D., Chamot, D., Fliegel, L. and Goss, G.** (2021). Rainbow Trout (Oncorhynchus mykiss) $Na^+/H^+$ Exchangers tNhe3a and tNhe3b Display Unique Inhibitory Profiles Dissimilar from Mammalian NHE Isoforms. *Int. J. Mol. Sci.* **22**, 2205.

**Bohr, C., Hasselbalch, K. and Krogh, A.** (1904). About a new biological relation of high importance that the blood carbonic acid tension exercises on its oxygen binding. *Skand. Arch. Physiol.* **16**, 402–412.

**Borgese, F., Garcia-Romeu, F. and Motais, R.** (1987). Ion movements and volume changes induced by catecholamines in erythrocytes of rainbow trout: effect of pH. *J. Physiol.* **382**, 145–157.

**Borgese, F., Sardet, C., Cappadoro, M., Pouyssegur, J. and Motais R** (1992). Cloning and expression of a cAMP-activated $Na^+/H^+$ exchanger: evidence that the cytoplasmic domain mediates hormonal regulation. *PNAS* **89**, 6765–9.

**Bourne, P. K. and Cossins, A. R.** (1982). On the instability of $K^+$ influx in erythrocytes of the rainbow trout, *Salmo gairdneri*, and the role of catecholamine hormones in maintaining *in vivo* influx activity. *J. Exp. Biol.* **101**, 93–104.

**Boutilier, R. G. and Ferguson, R. A.** (1989). Nucleated red cell function: metabolism and pH regulation. *Can. J. Zool.* **67**, 2986–2993.

**Boutilier, R. G., Heming, T. A. and Iwama, G. K.** (1984). Physicochemical parameters for use in fish respiratory physiology. In *Fish Physiology* (ed. Hoar W. S. and Randall, D. J.), pp. 403–426. New York: Academic Press.

**Brauner, C. J. and Wang, T.** (1997). The optimal oxygen equilibrium curve: a comparison between environmental hypoxia and anemia. *Am. Zool.* **37**, 101–108.

**Brauner, C. J., Gilmour, K. M. and Perry, S. F.** (1996). Effect of haemoglobin oxygenation on Bohr proton release and $CO_2$ excretion in the rainbow trout. *Resp. Physiol.* **106**, 65–70.

**Brauner, C. J., Thorarensen, H., Gallaugher, P., Farrell, A. P. and Randall, D. J.** (2000a). $CO_2$ transport and excretion in rainbow trout (*Oncorhynchus mykiss*) during graded sustained exercise. *Resp. Physiol.* **119**, 69–82.

**Brauner, C. J., Thorarensen, H., Gallaugher, P., Farrell, A. P. and Randall, D. J.** (2000b). The interaction between $O_2$ and $CO_2$ exchange in rainbow trout during graded sustained exercise. *Resp. Physiol.* **119**, 83–96.

**Brauner, C. J., Wang, T., Val, A. L. and Jensen, F. B.** (2001). Non-linear release of Bohr protons with haemoglobin-oxygenation in the blood of two teleost fishes; carp (*Cyprinus carpio*) and tambaqui (*Colossoma macropomum*). *Fish Physiol. Biochem.* **24**, 97–104.

**Brittain, T.** (1987). The Root effect. *Comp. Biochem. Physiol.* **86B**, 473–481.

**Bushnell, B.** (2014). *BBMap: A Fast, Accurate, Splice-Aware Aligner*. Lawrence Berkeley National Lab. (LBNL), Berkeley, CA (United States).

**Caldwell, S., Rummer, J. L. and Brauner, C. J.** (2006). Blood sampling techniques and storage duration: Effects on the presence and magnitude of the red blood cell beta-adrenergic response in rainbow trout (*Oncorhynchus mykiss*). *Comp. Biochem. Physiol., A: Mol. Integr. Physiol.* **144**, 188–195.

**Castresana, J.** (2000). Selection of Conserved Blocks from Multiple Alignments for Their Use in Phylogenetic Analysis. *Mol. Biol. Evol.* **17**, 540–552.

**Chen, X. L., Zhang, B., Chng, Y. R., Ong, J. L. Y., Chew, S. F., Wong, W. P., Lam, S. H. and Ip, Y. K.** (2017). $Na^+/H^+$ Exchanger 3 Is Expressed in Two Distinct Types of Ionocyte, and Probably Augments Ammonia Excretion in One of Them, in the Gills of the Climbing Perch Exposed to Seawater. *Front. Physiol.* **8**.

**Chen, S., Zhou, Y., Chen, Y. and Gu, J.** (2018). fastp: an ultra-fast all-in-one FASTQ preprocessor. *Bioinformatics* **34**, i884–i890.

**Clifford, A. M., Weinrauch, A. M., Edwards, S. L., Wilkie, M. P. and Goss, G. G.** (2017). Flexible ammonia handling strategies using both cutaneous and branchial epithelia in the highly ammonia-tolerant Pacific hagfish. *Am. J. Physiol. Regul., Integr. Comp. Physiol.* **313**, R78–R90.

**Cossins, A. R. and Richardson, P. A.** (1985). Adrenaline-induced $Na^+/H^+$ exchange in trout erythrocytes and its effects upon oxygen carrying capacity. *J. Exp. Biol.* **118**, 229–246.

**Damsgaard, C., Lauridsen, H., Harter, T. S., Kwan, G. T., Thomsen, J. S., Funder, A. M., Supuran, C. T., Tresguerres, M., Matthews, P. G. and Brauner, C. J.** (2020). A novel acidification mechanism for greatly enhanced oxygen supply to the fish retina. *eLife* **9**, e58995.

**Diaz, R. J. and Rosenberg, R.** (2008). Spreading Dead Zones and Consequences for Marine Ecosystems. *Science* **321**, 926–929.

**Dmitrieff, S., Alsina, A., Mathur, A. and Nédélec, F. J.** (2017). Balance of microtubule stiffness and cortical tension determines the size of blood cells with marginal band across species. *PNAS* 201618041.

**Dunn, C., O'Dowd, A. and Randall, R. E.** (1999). Fine mapping of the binding sites of monoclonal antibodies raised against the Pk tag. *J Immunol Methods* **224**, 141–150.

**Edgar, R. C.** (2004). MUSCLE: multiple sequence alignment with high accuracy and high throughput. *Nucleic Acids Res.* **32**, 1792–1797.

**Ferguson, R. A., Tufts, B. L. and Boutilier, R. G.** (1989). Energy metabolism in trout red cells: consequences of adrenergic stimulation *in vivo* and *in vitro*. *J. Exp. Biol.* **143**, 133–147.

**Frieder, C. A., Nam, S. H., Martz, T. R. and Levin, L. A.** (2012). High temporal and spatial variability of dissolved oxygen and pH in a nearshore California kelp forest. *Biogeosciences* **9**, 3917–3930.

**Galtier, N., Gouy, M. and Gautier, C.** (1996). SEAVIEW and PHYLO_WIN: two graphic tools for sequence alignment and molecular phylogeny. *Bioinformatics* **12**, 543–548.

**Gens, J. S., Du, H., Tackett, L., Kong, S.-S., Chu, S. and Montrose, M. H.** (2007). Different ionic conditions prompt NHE2 and NHE3 translocation to the plasma membrane. *Biochim. Biophys. Acta, Biomembr.* **1768**, 1023–1035.

**Gibson, J., Cossins, A. and Ellory, J.** (2000). Oxygen-sensitive membrane transporters in vertebrate red cells. *J. Exp. Biol.* **203**, 1395–1407.

**Gouy, M., Guindon, S. and Gascuel, O.** (2010). SeaView Version 4: A Multiplatform Graphical User Interface for Sequence Alignment and Phylogenetic Tree Building. *Mol. Biol. Evol.* **27**, 221–224.

**Grabherr, M. G., Haas, B. J., Yassour, M., Levin, J. Z., Thompson, D. A., Amit, I., Adiconis, X., Fan, L., Raychowdhury, R., Zeng, Q., et al.** (2011). Full-length transcriptome assembly from RNA-Seq data without a reference genome. *Nat. Biotechnol.* **29**, 644–652.

**Harley, C. D. G., Hughes, A. R., Hultgren, K. M., Miner, B. G., Sorte, C. J. B., Thornber, C. S., Rodriguez, L. F., Tomanek, L. and Williams, S. L.** (2006). The impacts of climate change in coastal marine systems. *Ecol. Lett.* **9**, 228–241.

**Hughes, G. M.** (1973). Respiratory responses to hypoxia in fish. *Am. Zool.* **13**, 475–489.

**Jacobs, M. H. and Stewart, D. R.** (1942). The role of carbonic anhydrase in certain ionic exchanges involving the erythrocyte. *J. gen. Physiol.* **25**, 539–552.

**Jensen, F. B. and Weber, R. E.** (1982). Respiratory properties of tench blood and hemoglobin. Adaptation to hypoxic-hypercapnic water. *Mol. Physiol.* **2**, 235–250.

**Jensen, B. J., Nikinmaa, M. and Weber, R. E.** (1983). Effects of exercise stress on acid-base balance and respiratory function in blood of the teleost *Tinca tinca*. *Resp. Physiol.* **51**, 291–301.

**Joseph-Silverstein, J. and Cohen, W. D.** (1984). The cytoskeletal system of nucleated erythrocytes. III. Marginal band function in mature cells. *J. Cell Biol.* **98**, 2118–2125.

**Kobayashi, M., Ishigaki, K., Kobyashi, M. and Imai, K.** (1994). Shape of the haemoglobin-oxygen equilibrium curve and oxygen transport efficiency. *Resp. Physiol.* **95**, 321–328.

**Kozak, M.** (1987). An analysis of 5'-noncoding sequences from 699 vertebrate messenger RNAs. *Nucleic Acids Res.* **15**, 8125–8148.

**Landau, M., Herz, K., Padan, E. and Ben-Tal, N.** (2007). Model structure of the $Na^+/H^+$ exchanger 1 (NHE1): functional and clinical implications. *J Biol Chem* **282**, 37854–37863.

**Lawrence, S. P., Holman, G. D. and Koumanov, F.** (2010). Translocation of the $Na^+/H^+$ exchanger 1 (NHE1) in cardiomyocyte responses to insulin and energy-status signalling. *Biochem J* **432**, 515–523.

**Le, S. Q. and Gascuel, O.** (2008). An Improved General Amino Acid Replacement Matrix. *Mol. Biol. Evol.* **25**, 1307–1320.

**Lee, B. L. L. L., Sykes, B. D. S. D. and Fliegel, L. F.** (2011). Structural analysis of the $Na^+/H^+$ exchanger isoform 1 (NHE1) using the divide and conquer approach. *Biochem. Cell Biol.*

**Lewis, E. and Wallace, D. W. R.** (1998). *Program Developed for CO2 System Calculations.* Oak Ridge Natl. Lab., Oak Ridge, Tenn.: ORNL/CDIAC-105, Carbon Dioxide Inf. Anal. Cent.

**Mahe, Y., Garciaromeu, F. and Motais, R.** (1985). Inhibition by amiloride of both adenylate-cyclase activity and the $Na^+/H^+$ antiporter in fish erythrocytes. *Eur. J. Pharmacol.* **116**, 199–206.

**Mairbäurl, H.** (1994). Red blood cell function in hypoxia at altitude and exercise. *Int. J. Sports Med.* **15**, 51–63.

**Mairbäurl, H. and Weber, R. E.** (2012). Oxygen transport by hemoglobin. *Compr. Physiol.* **2**, 1463–1489.

**Mandic, M., Todgham, A. E. and Richards, J. G.** (2009). Mechanisms and evolution of hypoxia tolerance in fish. *Proc. R. Soc. Lond., Ser. B: Biol. Sci.* **276**, 735–744.

**Miller, M. A., Pfeiffer, W. and Schwartz, T.** (2010). Creating the CIPRES Science Gateway for Inference of Large Phylogenetic Trees. pp. 1–8. New Orleans, LA.

**Montgomery, D. W., Simpson, S. D., Engelhard, G. H., Birchenough, S. N. R. and Wilson, R. W.** (2019). Rising $CO_2$ enhances hypoxia tolerance in a marine fish. *Sci. Rep.* **9**, 15152.

**Motais, R., Garcia-Romeu, F. and Borgese, F.** (1987). The control of $Na^+/H^+$ exchange by molecular oxygen in trout erythrocytes. A possible role of hemoglobin as a transducer. *J. gen. Physiol.* **90**, 197–207.

**Motais, R., Fievet, B., Garcia-Romeu, F. and Thomas, S.** (1989). $Na^+$-$H^+$ exchange and pH regulation in red blood cells: role of uncatalyzed $H_2CO_3^-$ dehydration. *Am. J. Physiol.* **256**, C728–C735.

**Nikinmaa, M.** (1983). Adrenergic regulation of hemoglobin oxygen-affinity in rainbow trout red cells. *J. Comp. Physiol.* **152**, 67–72.

**Nikinmaa, M.** (1992). Membrane transport and control of hemoglobin-oxygen affinity in nucleated erythrocytes. *Physiol. Rev.* **72**, 301–21.

**Nikinmaa, M. and Huestis, W. H.** (1984). Adrenergic swelling of nucleated erythrocytes - cellular mechanisms in a bird, domestic goose, and 2 teleosts, striped bass and rainbow trout. *J. Exp. Biol.* **113**, 215–224.

**Nikinmaa, M. and Soivio, A.** (1979). Oxygen dissociation curves and oxygen capacities of blood of a freshwater fish, *Salmo gairdneri*. *Ann. Zool. Fenn.* **16**, 217–221.

**Nikinmaa, M., Cech, J. J. and McEnroe, M.** (1984). Blood oxygen transport in stressed striped bass (*Morone saxatilis*): role of β-adrenergic responses. *J. Comp. Physiol.* **154**, 365–369.

**Nishikawa, T., Ota, T. and Isogai, T.** (2000). Prediction whether a human cDNA sequence contains initiation codon by combining statistical information and similarity with protein sequences. *Bioinformatics* **16**, 960–967.

**Parks, S. K., Tresguerres, M. and Goss, G. G.** (2007). Blood and gill responses to HCl infusions in the Pacific hagfish (*Eptatretus stoutii*). *Can. J. Zool.* **85**, 855–862.

**Pedersen, S. F., King, S. A., Rigor, R. R., Zhuang, Z., Warren, J. M. and Cala, P. M.** (2003). Molecular cloning of NHE1 from winter flounder RBCs: activation by osmotic shrinkage, cAMP, and calyculin A. *Am. J. Physiol. Cell Physiol.* **284**, C1561–C1576.

**Pelster, B.** (1997). Buoyancy at depth. In *Fish Physiology* (ed. Randall, D.) and Farrell, A.), pp. 195–238. New York: Academic Press.

**Pelster, B. and Randall, D. J.** (1998). Physiology of the Root effect. In *Fish Physiology* (ed. Perry, S. F.) and Tufts, B. L.), pp. 113–140. New York: Academic Press.

**Perutz, M. F. and Brunori, M.** (1982). Stereochemistry of cooperative effects in fish and amphibian haemoglobins. *Nature* **299**, 421–426.

**Randall, D. J. and Perry, S. F.** (1992). Catecholamines. In *Fish Physiology* (ed. Hoar, W. S.), Randall, D. J.), and Farrell, A. P.), pp. 255–300. New York: Academic Press.

**RCoreTeam** (2020). *R: A language and environment for statistical computing*. Vienna, Austria: R Foundation for Statistical Computing.

**Root, R. W.** (1931). The respiratory function of the blood of marine fishes. *Biol. Bull.* **61**, 427–456.

**RStudioTeam** (2021). *RStudio: Integrated Development Environment for R*. Boston, MA: RStudio, Inc.

**Rummer, J. L. and Brauner, C. J.** (2015). Root effect haemoglobins in fish may greatly enhance general oxygen delivery relative to other vertebrates. *PloS one* **10**, e0139477.

**Rummer, J. L., Roshan-Moniri, M., Balfry, S. K. and Brauner, C. J.** (2010). Use it or lose it? Sablefish, *Anoplopoma fimbria*, a species representing a fifth teleostean group where the βNHE associated with the red blood cell adrenergic stress response has been secondarily lost. *J. Exp. Biol.* **213**, 1503–1512.

**Salama, A. and Nikinmaa, M.** (1988). The adrenergic responses of carp (*Cyprinus carpio*) red cells: effects of $PO_2$ and pH. *J. Exp. Biol.* **136**, 405–416.

**Salama, A. and Nikinmaa, M.** (1989). Species differences in the adrenergic responses of fish red cells: studies on whitefish, pikeperch, trout and carp. *Fish Physiol. Biochem.* **6**, 167–173.

**Scholander, P. F. and Van Dam, L.** (1954). Secretion of gases against high pressures in the swimbladder of deep sea fishes. I. Oxygen dissociation in blood. *Biol. Bull.* **107**, 247–259.

**Shu, J. J., Harter, T. S., Morrison, P. R. and Brauner, C. J.** (2017). Enhanced hemoglobin-oxygen unloading in migratory salmonids. *J. Comp. Physiol. B* **7**, 1–11.

**Stamatakis, A.** (2014). RAxML version 8: a tool for phylogenetic analysis and post-analysis of large phylogenies. *Bioinformatics* **30**, 1312–1313.

**Talavera, G. and Castresana, J.** (2007). Improvement of Phylogenies after Removing Divergent and Ambiguously Aligned Blocks from Protein Sequence Alignments. *Systematic Biology* **56**, 564–577.

**Tenney, S. M.** (1995). Hypoxia and the Brain: Functional significance of differences in mammalian hemoglobin affinity for oxygen. In *Proceeding of the 9th International Hypoxia Symposium* (ed. Sutton, J. R, Houston C. S., and Coates, G.), pp. 57–68. Lake Louise, Canada: Queen city printers, Burlington, Vt.

**Tetens, V. and Lykkeboe, G.** (1988). Potency of adrenaline and noradrenaline for b-adrenergic proton extrusion from red cells of rainbow trout, *Salmo gairdneri*. *J. Exp. Biol.* **134**, 267–280.

**Van Dolah, F M** (2000). Marine algal toxins: origins, health effects, and their increased occurrence. *Environ. Health Perspect.* **108**, 133–141.

**van Kampen, E. J. and Zijlstra, W. G.** (1983). Spectrophotometry of Hemoglobin and Hemoglobin Derivatives. In *Advances in Clinical Chemistry* (ed. Latner, A. L.) and Schwartz, M. K.), pp. 199–257. Elsevier.

**Vaquer-Sunyer, R. and Duarte, C. M.** (2008). Thresholds of hypoxia for marine biodiversity. *PNAS* **105**, 15452–15457.

**Weaver, Y. R., Kiessling, K. and Cossins, A. R.** (1999). Responses of the $Na^+/H^+$ exchanger of European flounder red blood cells to hypertonic, beta-adrenergic and acidotic stimuli. *J. Exp. Biol.* **202**, 21–32.

**Wickham, H.** (2009). *ggplot2: Elegant Graphics for Data Analysis*. New York: Springer-Verlag.

**Wittenberg, J. B. and Wittenberg, B. A.** (1962). Active secretion of oxygen into the eye of fish. *Nature* **194**, 106–107.

**Wood, C. M., McDonald, D. G. and McMahon, B. R.** (1982). The influence of experimental anemia on blood acid-base regulation *in vivo* and *in vitro* in the starry flounder (*Platichthys stellatus*) and the rainbow trout (*Salmo gairdneri*). *J. Exp. Biol.* **96**, 221–237.

**Zeidler, R. and Kim, H. D.** (1977). Preferential hemolysis of postnatal calf red cells induced by internal alkalinization. *J. Gen. Physiol.* **70**, 385–401.

**Zhao, H., Shiue, H., Palkon, S., Wang, Y., Cullinan, P., Burkhardt, J. K., Musch, M. W., Chang, E. B. and Turner, J. R.** (2004). Ezrin regulates NHE3 translocation and activation after $Na^+$-glucose cotransport. *PNAS* **101**, 9485–9490.

## Figure legends

**Figure 1 Oxygen binding characteristics of white seabass whole blood.** Oxygen equilibrium curves showing haemoglobin-oxygen saturation (Hb-$O_2$ sat.; %) as a function of the partial pressure of oxygen ($PO_2$; mmHg, where 7.5 mmHg equals 1%) at five partial pressures of carbon dioxide ($PCO_2$). The $PO_2$ that yields 50% Hb-$O_2$ saturation ($P_{50}$) and the cooperativity coefficient of Hb-$O_2$ binding (Hill coefficient, $n_H$) are shown for each curve. The main effects of $PCO_2$ on $P_{50}$ and $n_H$ were analysed with ACOVA ($P < 0.05$, $N = 8$). The Bohr coefficients (B) relative to extracellular ($pH_e$) and intracellular ($pH_i$), the relationship between $pH_e$ and $pH_i$ and the non-bicarbonate buffer capacity of the blood (at 5% Hct) were determined by linear regressions (see Fig. S1). The Root effect (R) was determined at 21% $PO_2$ from the model parameters shown for the DMSO treatment in Fig. 6B. All data are means±s.e.m.

**Figure 2 Changes in blood parameters after adrenergic stimulation of white seabass whole blood.** A) Haematocrit (%), B) mean cell haemoglobin content (MCHC; mM haemoglobin $l^{-1}$ red blood cells), C) extracellular pH ($pH_e$) and D) intracellular pH ($pH_i$). Blood was equilibrated in tonometers at 3% $PO_2$ and 1% $PCO_2$ and treated with either: i) a carrier control (DMSO; 0.25%), ii) the β-adrenergic agonist isoproterenol (ISO; 10 µM) or iii) ISO plus amiloride (ISO+Am; 1 mM), an inhibitor of sodium-proton exchangers (NHE). The dotted line indicates initial values for each parameter and changes were recorded over 60 min. The main effects of drug, time, and their interaction term (drug×time) were analysed with a two-way ANOVA ($P < 0.05$, $N = 6$ and $N = 5$ for ISO+Am). There were no significant changes in haemoglobin concentration ([Hb]; mM) throughout the trials. Multiple comparisons were with paired t-tests with a Benjamini-Hochberg correction and superscript letters that differ indicate significant differences between treatments at 60 min. Individual datapoints and means±s.e.m. Inserts E-H) differential interference contrast (DIC, 60x) images of red blood cells fixed at the beginning (ini) and the end of the trial (T60). Cell swelling was visually confirmed in ISO-treated cells, but not in other treatments, and mostly along the z-axis of the cells (arrows), while the x-y-axis seemed largely unaffected.

**Figure 3: Phylogenetic analysis of nine NHE-like protein sequences in the *de novo* assembly of a combined white seabass gill and red blood cell transcriptome.** Novel white seabass sequences are highlighted in blue and the β-NHE in red (Slc9a1b). Shadings delineate sub-families of the Slc9a1 gene family. The tree was rooted against the NHE2 from *Caenorhabditis elegans* in orange. Accession numbers for all species are those reported in Table S1.

**Figure 4 Immunocytochemical localisation of the β-adrenergic sodium proton exchanger (β-NHE) in white seabass red blood cells.** Blood was equilibrated in tonometers at 3% $PO_2$ and 1% $PCO_2$ for 60 mins (see Fig. 2 for details) in the presence of either: A-D) a carrier control (DMSO; 0.25%), or E-H) the β-adrenergic agonist isoproterenol (ISO; 10 µM). Fixed cells were immuno-stained with a monoclonal α-tubulin antibody to visualize the marginal band (red), with DAPI to visualize the cell nuclei (A and E), and with a polyclonal anti-β-NHE antibody (green,

B and F). D and H) Magnified view of the insets in the merged images, where arrows indicate weak or absent β-NHE immunoreactivity on the membrane of Ctrl cells and intense staining in ISO-treated cells (for a larger sample size of these representative patters see Fig. S3).

**Figure 5 Haemoglobin-oxygen saturation (Hb-$O_2$ sat.; %) during hypercapnic acidification of white seabass whole blood.** Haematocrit was set to 5%, blood was equilibrated in tonometers at 21% $PO_2$ and 0.3% $PCO_2$ and treated with either: i) a carrier control (DMSO; 0.25%), ii) the β-adrenergic agonist isoproterenol (ISO; 10 µM), or iii) ISO plus amiloride (ISO+Am; 1 mM), an inhibitor of sodium-proton exchangers (NHE). For each sample, runs were performed in normoxia (21% $PO_2$; solid symbols) or hypoxia (3% $PO_2$; open symbols). Individual datapoints and means±s.e.m. ($N$ = 6).

**Figure 6 Parameter estimates describing the changes in haemoglobin-oxygen saturation during hypercapnic acidification of white seabass whole blood.** A) The $PCO_2$ that elicits a half-maximal reduction in Hb-$O_2$ saturation ($EC_{50}PCO_2$; %). and B) the maximal reduction in Hb-$O_2$ saturation due to acidification (Max. ΔHb-$O_2$ sat.; %). Treatments were: i) a carrier control (DMSO; 0.25%), ii) the β-adrenergic agonist isoproterenol (ISO; 10 µM), or iii) ISO plus amiloride (ISO+Am; 1 mM) an inhibitor of sodium-proton exchangers (NHE). For each sample, runs were performed in normoxia (21% $PO_2$; solid symbols) or hypoxia (3% $PO_2$; open symbols). The main effects of drug treatments (drug), oxygen ($O_2$) and their interaction term (drug×$O_2$) were analysed with a two-way ANOVA ($P < 0.05$, $N$ = 6). Multiple comparisons were with paired t-tests and a Benjamini-Hochberg correction and superscript letters that differ indicate significant differences between treatments for each $O_2$ tension. Individual datapoints and means±s.e.m. ($N$ = 6).

**Figure 7 Relative changes in haemoglobin-oxygen saturation (ΔHb-$O_2$ sat.; %) during hypercapnic acidification of white seabass whole blood.** A) in normoxia (21% $PO_2$; solid symbols) or B) in hypoxia (3% $PO_2$; open symbols). Treatments were: i) a carrier control (DMSO; 0.25%), ii) the β-adrenergic agonist isoproterenol (ISO; 10 µM), or iii) ISO plus amiloride (ISO+Am; 1 mM), an inhibitor of sodium-proton exchangers (NHE). Individual datapoints, means±s.e.m. and 95% confidence intervals ($N$ = 6).

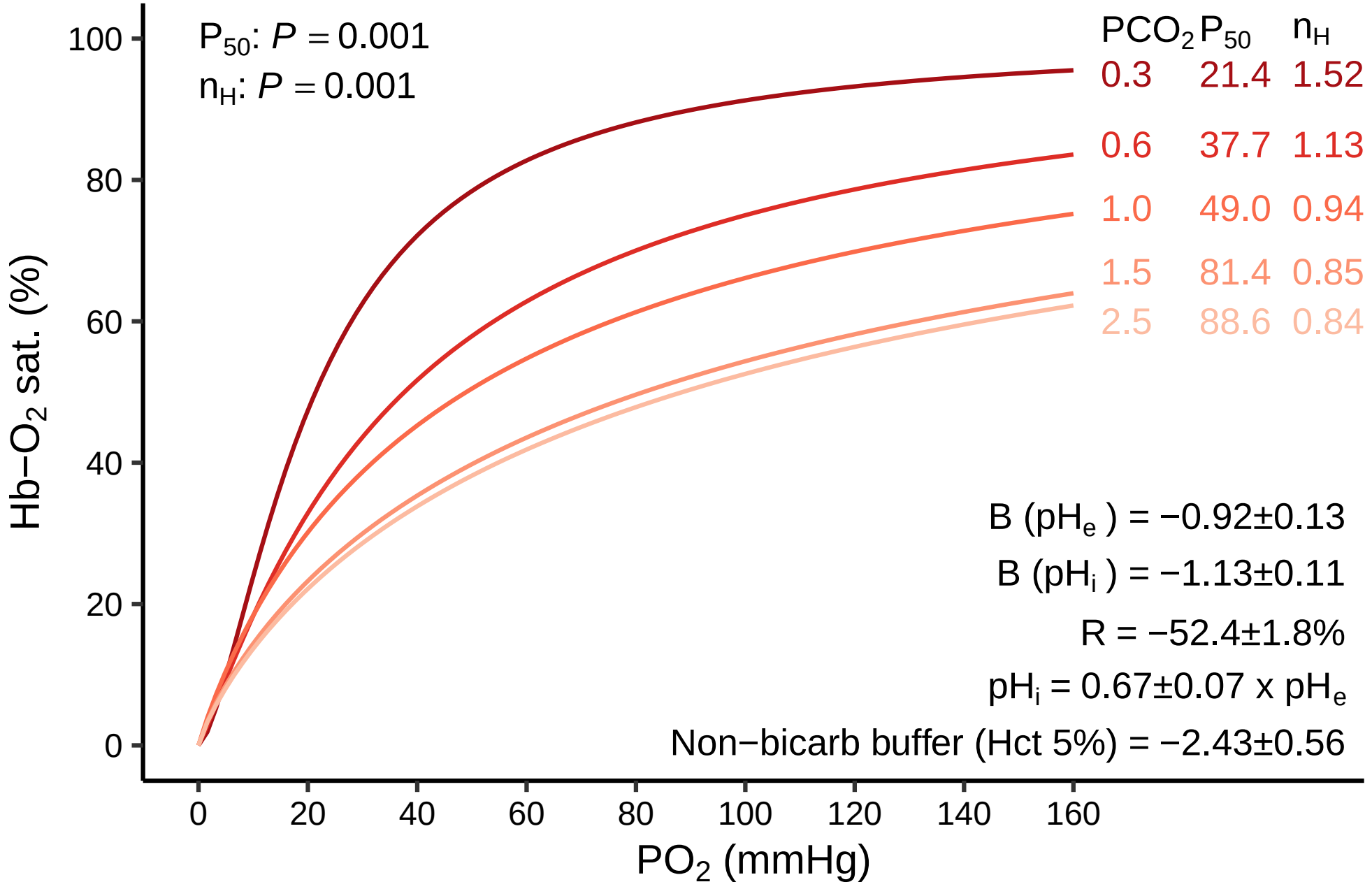
P50: P = 0.001
nH: P = 0.001
PCO2 P50 nH
0.3 21.4 1.52
0.6 37.7 1.13
1.0 49.0 0.94
1.5 81.4 0.85
2.5 88.6 0.84
B (pHe ) = −0.92±0.13
B (pHi ) = −1.13±0.11
R = −52.4±1.8%
pHi = 0.67±0.07 x pHe
Non−bicarb buffer (Hct 5%) = −2.43±0.56
Hb−O2 sat. (%)
PO2 (mmHg)
0
20
40
60
80
100
120
140
160

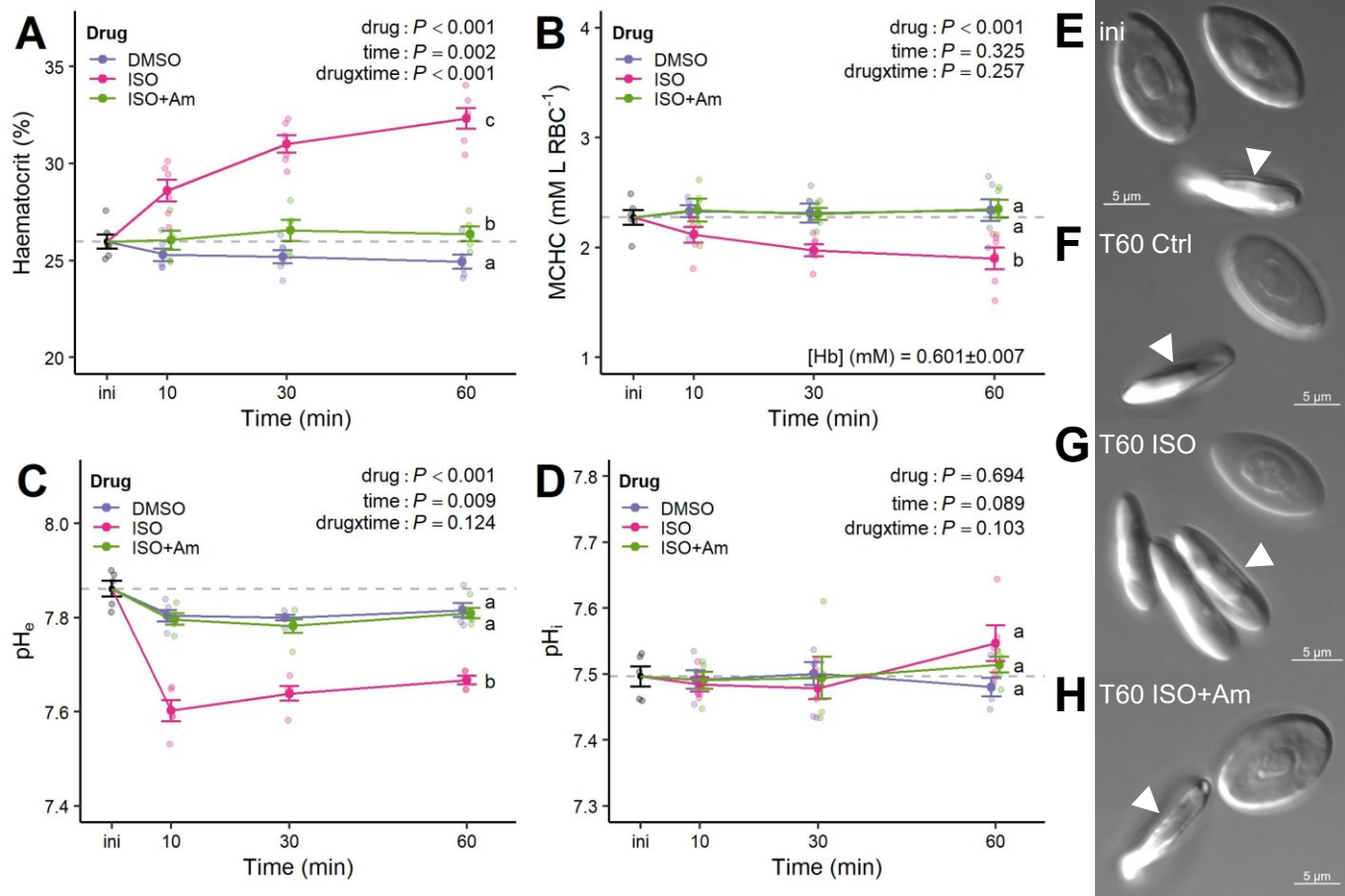
A
Drug
DMSO
ISO
ISO+Am
drug : P < 0.001
time : P = 0.002
drugxtime : P < 0.001
Haematocrit (%)
35
30
25
20
c
b
a
ini
10
30
60
Time (min)
B
Drug
DMSO
ISO
ISO+Am
drug : P < 0.001
time : P = 0.325
drugxtime : P = 0.257
MCHC (mM L RBC-1)
4
3
2
1
a
a
b
[Hb] (mM) = 0.601±0.007
ini
10
30
60
Time (min)
C
Drug
DMSO
ISO
ISO+Am
drug : P < 0.001
time : P = 0.009
drugxtime : P = 0.124
pHe
8.0
7.8
7.6
7.4
a
a
b
ini
10
30
60
Time (min)
D
Drug
DMSO
ISO
ISO+Am
drug : P = 0.694
time : P = 0.089
drugxtime : P = 0.103
pHi
7.8
7.7
7.6
7.5
7.4
7.3
a
a
a
ini
10
30
60
Time (min)
E
ini
5 µm
F
T60 Ctrl
5 µm
G
T60 ISO
5 µm
H
T60 ISO+Am
5 µm

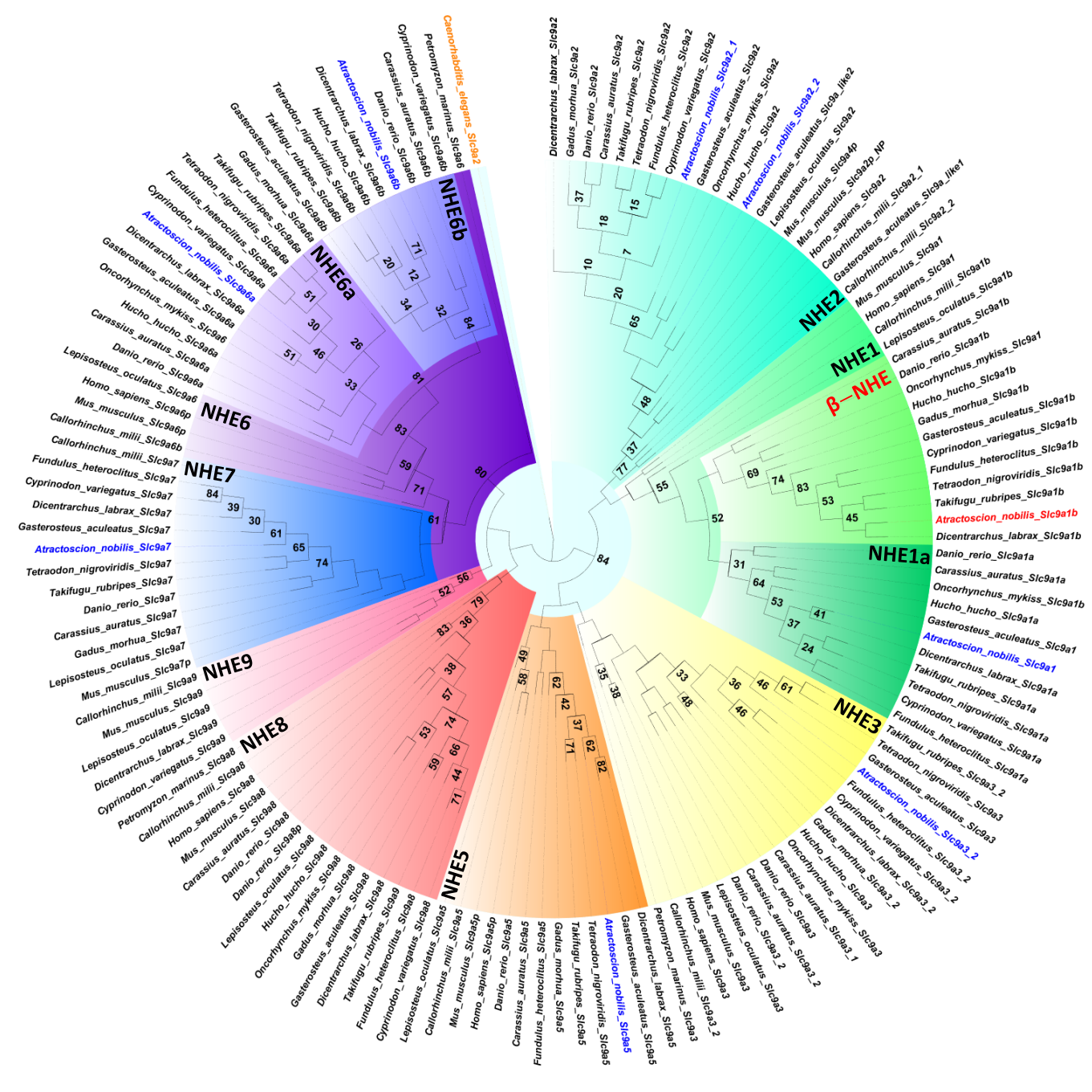
NHE1
NHE2
β–NHE
NHE1a
NHE3
NHE5
NHE8
NHE9
NHE7
NHE6
NHE6a
NHE6b
Dicentrarchus_labrax_Slc9a2
Gadus_morhua_Slc9a2
Danio_rerio_Slc9a2
Carassius_auratus_Slc9a2
Takifugu_rubripes_Slc9a2
Tetraodon_nigroviridis_Slc9a2
Fundulus_heteroclitus_Slc9a2
Cyprinodon_variegatus_Slc9a2
Atractoscion_nobilis_Slc9a2_1
Gasterosteus_aculeatus_Slc9a2
Oncorhynchus_mykiss_Slc9a2
Atractoscion_nobilis_Slc9a2_2
Hucho_hucho_Slc9a2
Gasterosteus_aculeatus_Slc9a_like2
Lepisosteus_oculatus_Slc9a2
Mus_musculus_Slc9a4p
Homo_sapiens_Slc9a2p_NP
Callorhinchus_milii_Slc9a2_1
Gasterosteus_aculeatus_Slc9a_like1
Callorhinchus_milii_Slc9a2_2
Gasterosteus_aculeatus_Slc9a1
Callorhinchus_milii_Slc9a1
Mus_musculus_Slc9a1
Homo_sapiens_Slc9a1
Callorhinchus_milii_Slc9a1b
Lepisosteus_oculatus_Slc9a1b
Carassius_auratus_Slc9a1b
Danio_rerio_Slc9a1b
Oncorhynchus_mykiss_Slc9a1
Hucho_hucho_Slc9a1b
Gadus_morhua_Slc9a1b
Gasterosteus_aculeatus_Slc9a1b
Cyprinodon_variegatus_Slc9a1b
Fundulus_heteroclitus_Slc9a1b
Tetraodon_nigroviridis_Slc9a1b
Takifugu_rubripes_Slc9a1b
Atractoscion_nobilis_Slc9a1b
Dicentrarchus_labrax_Slc9a1b
Danio_rerio_Slc9a1a
Carassius_auratus_Slc9a1a
Oncorhynchus_mykiss_Slc9a1b
Hucho_hucho_Slc9a1a
Gasterosteus_aculeatus_Slc9a1
Atractoscion_nobilis_Slc9a1
Dicentrarchus_labrax_Slc9a1a
Takifugu_rubripes_Slc9a1a
Tetraodon_nigroviridis_Slc9a1a
Cyprinodon_variegatus_Slc9a1a
Fundulus_heteroclitus_Slc9a1a
Takifugu_rubripes_Slc9a3_2
Tetraodon_nigroviridis_Slc9a3
Gasterosteus_aculeatus_Slc9a3
Atractoscion_nobilis_Slc9a3_2
Fundulus_heteroclitus_Slc9a3_2
Cyprinodon_variegatus_Slc9a3_2
Dicentrarchus_labrax_Slc9a3_2
Gadus_morhua_Slc9a3_2
Hucho_hucho_Slc9a3
Oncorhynchus_mykiss_Slc9a3_1
Carassius_auratus_Slc9a3_2
Danio_rerio_Slc9a3_2
Lepisosteus_oculatus_Slc9a3
Mus_musculus_Slc9a3
Homo_sapiens_Slc9a3_2
Callorhinchus_milii_Slc9a3_2
Petromyzon_marinus_Slc9a3
Dicentrarchus_labrax_Slc9a5
Gasterosteus_aculeatus_Slc9a5
Atractoscion_nobilis_Slc9a5
Tetraodon_nigroviridis_Slc9a5
Takifugu_rubripes_Slc9a5
Gadus_morhua_Slc9a5
Danio_rerio_Slc9a5
Carassius_auratus_Slc9a5
Fundulus_heteroclitus_Slc9a5
Cyprinodon_variegatus_Slc9a5
Lepisosteus_oculatus_Slc9a5
Callorhinchus_milii_Slc9a5
Mus_musculus_Slc9a5p
Homo_sapiens_Slc9a5p
Danio_rerio_Slc9a8
Carassius_auratus_Slc9a8
Lepisosteus_oculatus_Slc9a8
Hucho_hucho_Slc9a8
Oncorhynchus_mykiss_Slc9a8
Gadus_morhua_Slc9a8
Gasterosteus_aculeatus_Slc9a8
Dicentrarchus_labrax_Slc9a8
Takifugu_rubripes_Slc9a8
Fundulus_heteroclitus_Slc9a8
Cyprinodon_variegatus_Slc9a8
Lepisosteus_oculatus_Slc9a8
Callorhinchus_milii_Slc9a8
Homo_sapiens_Slc9a8
Mus_musculus_Slc9a8
Carassius_auratus_Slc9a8
Danio_rerio_Slc9a8p
Lepisosteus_oculatus_Slc9a9
Hucho_hucho_Slc9a9
Oncorhynchus_mykiss_Slc9a9
Gadus_morhua_Slc9a9
Gasterosteus_aculeatus_Slc9a9
Dicentrarchus_labrax_Slc9a9
Takifugu_rubripes_Slc9a9
Fundulus_heteroclitus_Slc9a9
Cyprinodon_variegatus_Slc9a9
Lepisosteus_oculatus_Slc9a9
Dicentrarchus_labrax_Slc9a9
Cyprinodon_variegatus_Slc9a9
Petromyzon_marinus_Slc9a9
Callorhinchus_milii_Slc9a9
Mus_musculus_Slc9a9
Callorhinchus_milii_Slc9a9
Mus_musculus_Slc9a9p
Lepisosteus_oculatus_Slc9a9p
Gadus_morhua_Slc9a9p
Carassius_auratus_Slc9a9p
Danio_rerio_Slc9a9p
Takifugu_rubripes_Slc9a9p
Tetraodon_nigroviridis_Slc9a9p
Gasterosteus_aculeatus_Slc9a9p
Oncorhynchus_mykiss_Slc9a9p
Hucho_hucho_Slc9a9p
Atractoscion_nobilis_Slc9a9p
Dicentrarchus_labrax_Slc9a9p
Fundulus_heteroclitus_Slc9a9p
Cyprinodon_variegatus_Slc9a9p
Petromyzon_marinus_Slc9a9p
Caenorhabditis_elegans_Slc9a2
Cyprinodon_variegatus_Slc9a6b
Carassius_auratus_Slc9a6b
Danio_rerio_Slc9a6b
Dicentrarchus_labrax_Slc9a6b
Atractoscion_nobilis_Slc9a6b
Hucho_hucho_Slc9a6b
Tetraodon_nigroviridis_Slc9a6b
Takifugu_rubripes_Slc9a6b
Gasterosteus_aculeatus_Slc9a6a
Gadus_morhua_Slc9a6a
Takifugu_rubripes_Slc9a6a
Tetraodon_nigroviridis_Slc9a6a
Fundulus_heteroclitus_Slc9a6a
Cyprinodon_variegatus_Slc9a6a
Atractoscion_nobilis_Slc9a6a
Dicentrarchus_labrax_Slc9a6a
Gasterosteus_aculeatus_Slc9a6a
Oncorhynchus_mykiss_Slc9a6
Hucho_hucho_Slc9a6a
Carassius_auratus_Slc9a6a
Danio_rerio_Slc9a6a
Lepisosteus_oculatus_Slc9a6
Homo_sapiens_Slc9a6p
Mus_musculus_Slc9a6p
Callorhinchus_milii_Slc9a6b
Callorhinchus_milii_Slc9a7
Fundulus_heteroclitus_Slc9a7
Cyprinodon_variegatus_Slc9a7
Dicentrarchus_labrax_Slc9a7
Gasterosteus_aculeatus_Slc9a7
Atractoscion_nobilis_Slc9a7
Tetraodon_nigroviridis_Slc9a7
Takifugu_rubripes_Slc9a7
Danio_rerio_Slc9a7
Carassius_auratus_Slc9a7
Gadus_morhua_Slc9a7
Lepisosteus_oculatus_Slc9a7p
Mus_musculus_Slc9a7p

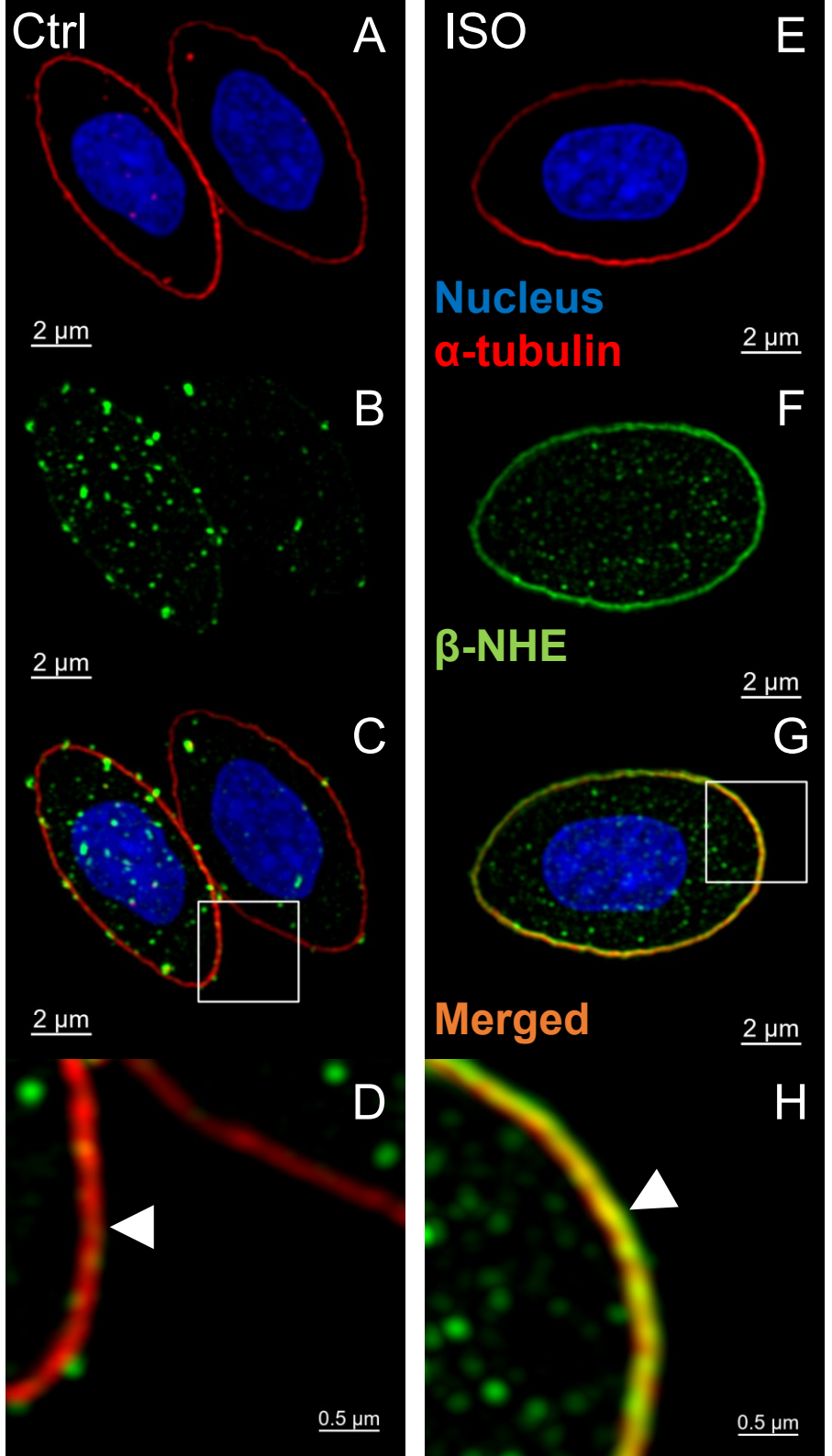
Ctrl
A
2 µm
B
2 µm
C
2 µm
D
0.5 µm
ISO
E
Nucleus
α-tubulin
2 µm
F
β-NHE
2 µm
G
Merged
2 µm
H
0.5 µm

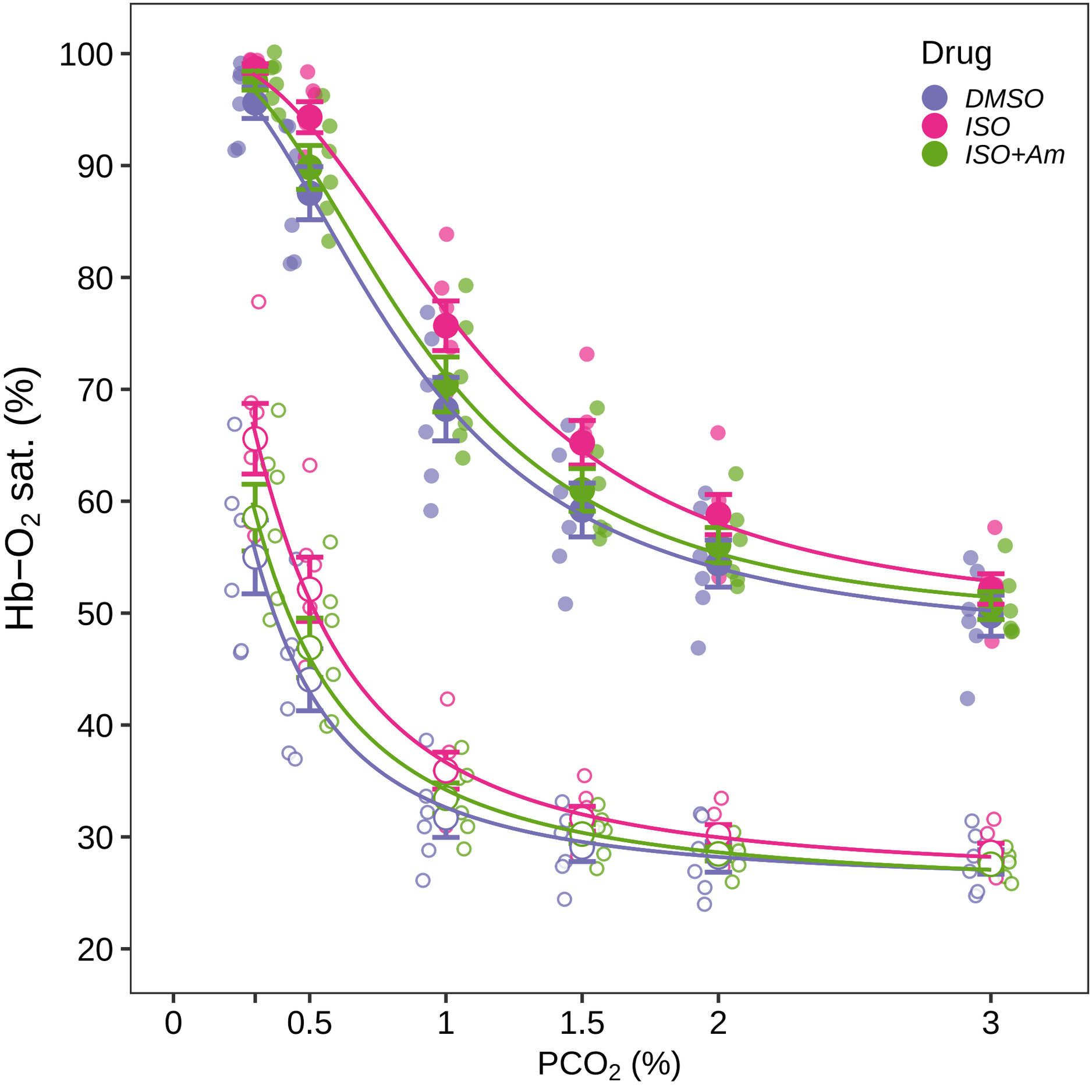
Drug
DMSO
ISO
ISO+Am
Hb–O2 sat. (%)
100
90
80
70
60
50
40
30
20
0
0.5
1
1.5
2
3
PCO2 (%)

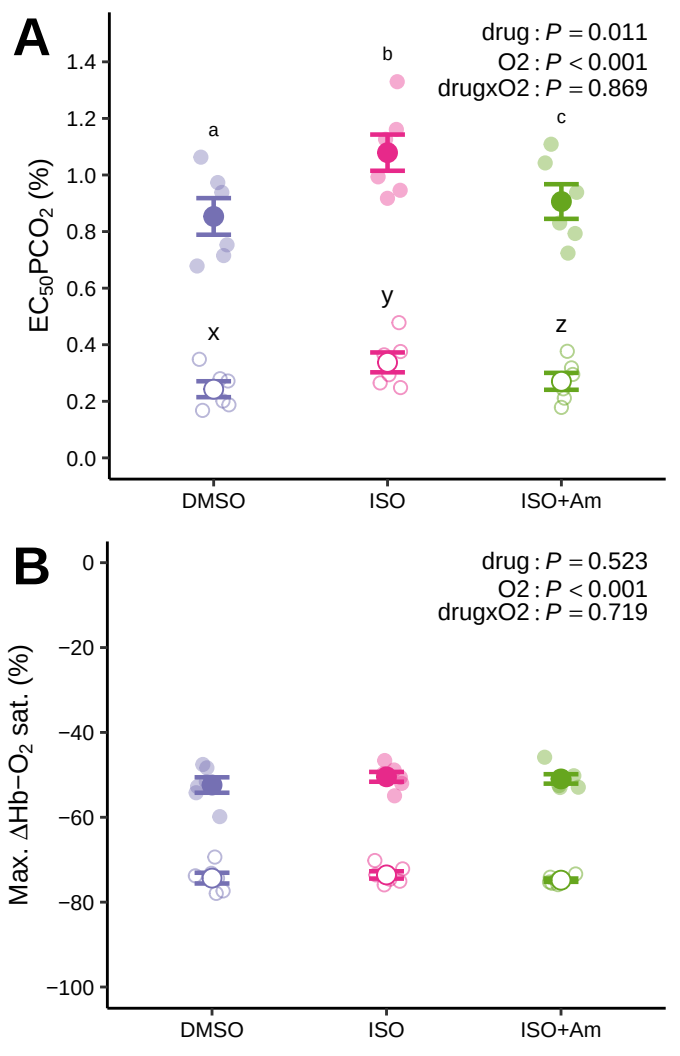
A
drug : P = 0.011
O2 : P < 0.001
drugxO2 : P = 0.869
EC50PCO2 (%)
1.4
1.2
1.0
0.8
0.6
0.4
0.2
0.0
a
b
c
x
y
z
DMSO
ISO
ISO+Am
B
drug : P = 0.523
O2 : P < 0.001
drugxO2 : P = 0.719
Max. ΔHb−O2 sat. (%)
0
−20
−40
−60
−80
−100
DMSO
ISO
ISO+Am

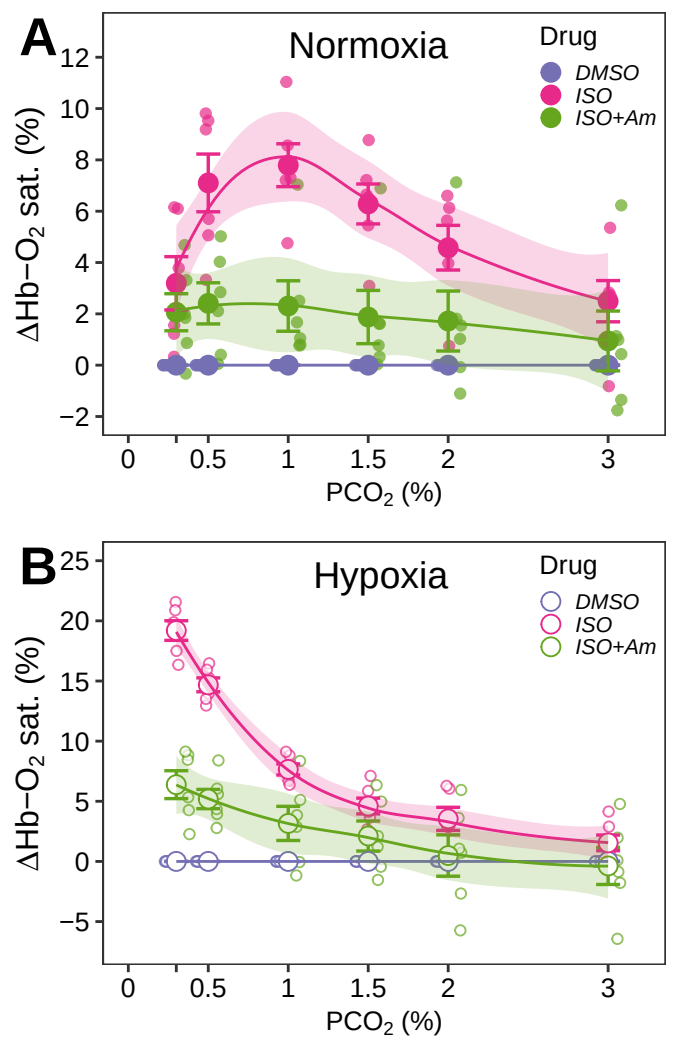
A
Normoxia
Drug
DMSO
ISO
ISO+Am
ΔHb−O2 sat. (%)
PCO2 (%)
B
Hypoxia
Drug
DMSO
ISO
ISO+Am
ΔHb−O2 sat. (%)
PCO2 (%)